

Theory of nonionic hydrophobic solutes in mixture solvent: Solvent-mediated interaction and solute-induced phase separation

Ryuichi Okamoto^a and Akira Onuki^b
^a *Research Institute for Interdisciplinary Science,
Okayama University, Okayama 700-8530, Japan*
^b *Department of Physics,
Kyoto University, Kyoto 606-8502, Japan*

(Dated: June 18, 2018)

We present a theory of nonionic solutes in a mixture solvent composed of water-like and alcohol-like species. First, we show relationship among the solvation chemical potential, the partial volumes v_i , the Kirkwood-Buff integrals, the second osmotic virial coefficient, and the Gibbs transfer free energy. We examine how the solute density n_3 is coupled to the solvent densities n_1 and n_2 in thermodynamics. In the limit of small compressibility, we show that the space-filling condition $\sum_i v_i n_i = 1$ nearly holds for inhomogeneous densities n_i , where the concentration fluctuations of the solvent can give rise to a large solute-solute attractive interaction. We also derive a solute spinodal density n_3^{sp1} for solute-induced instability. Next, we examine gas-liquid and liquid-liquid phase transitions induced by a small amount of a solute using the Mansoori, Carnahan, Starling, and Leland model for hard-sphere mixtures [J. Chem. Phys. **54**, 1523 (1971)]. Here, we assume that the solvent is close to its gas-liquid coexistence and the solute interacts repulsively with the water-like species but attractively with the alcohol-like one. We calculate the binodal and spinodal curves in the phase diagrams and examine nucleation for these two phase transitions.

I. INTRODUCTION

Long-standing research has been made on the role of hydrotropes in aqueous mixtures. Short-chain alcohols (such as methanol or tertiary butyl alcohol (TBA)) are typical examples of nonionic hydrotropes, which have an amphiphilic character but form no ordered structures in water due to their small sizes^{1,2}. A hydrotrope interacts with both water and hydrophobic solutes attractively, so it can improve the solute solubility as a cosolvent. As a unique effect, microemulsion-like droplets with radii of order $10^2 - 10^3$ nm emerge in ternary mixtures of water, alcohol, and a hydrophobic solute³⁻¹⁵ as well as macroscopic domains, depending on the solute and alcohol fractions. The former have well-defined interfaces yielding the Porod tail in the scattering amplitude⁶. This phenomenon is known by the name of *Ouzo effect*⁵. In such phase separation, a hydrophobic solute is accompanied by alcohol (as they go out of the original liquid) and the surface tension is considerably decreased due to interfacial adsorption of alcohol^{2,7,10,12,15}. Furthermore, scattering experiments⁸⁻¹¹ have indicated the presence of nanometer-sized, micelle-like aggregates¹⁶ in a wider *pre-Ouzo* region outside the binodal. In molecular dynamics simulation on water-ethanol-octanol mixtures^{8,11}, a large fraction of octanol molecules aggregate to form the cores of such nanoclusters, where a large number of ethanol molecules cover and penetrate these clusters.

In this paper, we theoretically treat a ternary mixture of a water-like solvent, an alcohol-like cosolvent, and a nonionic hydrophobic solute. We need to properly account for the steric and attractive interactions between the solute and the two solvent species at very small solute fractions. To this end, we use a continuum model of

hard-sphere mixtures by Mansoori, Carnahan, Starling, and Leland (MCSL)¹⁷, which is a generalization of the Carnahan and Starling model of one-component hard-spheres (CS)¹⁸. For simplicity, we assume attractive interactions in the van der Waals form, so we do not treat the hydrogen bonding among constituent protons and oxygens. We also do not include a surface-active character of the cosolvent, which leads to a reduction of the surface tension. In this scheme, we can examine how the selective solvation depends on the hard-sphere diameters, the attractive interaction parameters, and the compositions.

Our model solvent is assumed to be close to its gas-liquid coexistence, which is the case for water-alcohol mixtures. We use solutes which interact with the two solvent species very differently. In this situation, we encounter solute-induced gas-liquid and liquid-liquid phase transitions. In the former, the expelled solute particles form a gas at low pressures in the absence of appreciable solute-solute attractive interaction. The latter occurs when the attractive interaction between the solute and the second species is sufficiently strong. We examine two-phase coexistence, metastability, and instability for these phase transitions. We argue that the nucleation rate for the liquid-liquid transition is much larger than that for the gas-liquid one in the bulk in mixtures of water, alcohol, and a hydrophobic solute.

As a mysterious phenomenon, long-lived mesoscopic heterogeneities (presumably phase-separated domains) have been detected at very small fractions by dynamic light scattering, which emerge with addition of a small amount of a salt, a polymer, or a hydrophobic compound in one-phase states of aqueous mixtures or polymer solutions^{13,19-27}. From their diffusion constants, their sizes were in the range $10^2 - 10^3$ nm. Such precip-

itation occurs for various combinations of a solute and a mixture solvent, so it should generally originate from selective solvation of a solute^{28,29}.

As a well-known solute-induced gas-liquid transition, we mention formation of nanobubbles with dissolution of gases such as O₂, H₂, and Ar in ambient water^{30–35}. For example, Ohgaki *et al.*³¹ realized bubbles of such gases with radius 50 nm and volume fraction 0.01 in quasi-steady states, where bubble coalescence was suppressed by salts added. Such bulk nanobubbles are usually produced by breakup of large bubbles, while surface nanobubbles on hydrophobic walls can appear via heterogeneous nucleation. In this problem, it is crucial that ambient water is very close to its gas-liquid coexistence. Then, we can explain the bubble stability by including the Gibbs transfer free energy in the bubble free energy provided that the solute-water attractive interaction is weaker than that among the water molecules^{36,37}.

In the literature^{38–43}, much attention has also been paid to assembly of strongly hydrophobic particles in ambient water, where the proximity to gas-liquid coexistence is crucial³⁹. In our viewpoint, it can be treated as phase separation, since associated clusters should grow if their sizes exceed a critical size. However, this phenomenon has been studied only at its inception.

Before discussing phase separation, we present a statistical-mechanical theory of solvation in ternary mixtures. We relate the solvation chemical potential to various physical quantities including the partial volumes v_i ($i = 1, 2, 3$). For inhomogeneous densities n_i , we discuss how the space-filling condition $\sum_i v_i n_i = 1$ is nearly satisfied at long wavelengths in the limit of small compressibility. Namely, in nearly incompressible fluid mixtures, the deviations of $\sum_i v_i n_i$ from 1 should be small^{44,45}, while the concentration fluctuations can be enhanced due to molecular clustering. This is the case for water-alcohol mixtures. Then, the solvent-mediated, solute-solute interaction arises mostly from the solute-concentration coupling for not small cosolvent fractions.

The organization of this paper is as follows. In Sec. II, we will present the theoretical background of ternary mixtures. In Sec. III, we will use the MCSL model to investigate the solvation effects. In Sec. IV, we will examine the phase separation. Additionally, we will summarize the theory of the partial volumes and the Kirkwood-Buff integrals in Appendix A, examine the solute-induced gas-liquid transition in a one-component solvent in Appendix B, and present details of the CS model in Appendix C and MCSL model in Appendix D.

II. DILUTE SOLUTE IN MIXTURE SOLVENT

We consider nonionic ternary fluid mixtures. As a mixture solvent, we consider a water-like species (called water) ($i = 1$) and a cosolvent ($i = 2$). We then add a dilute solute ($i = 3$). Their densities are written as n_i . The sol-

vent composition (cosolvent molar fraction) is written as

$$X = n_2 / (n_1 + n_2). \quad (1)$$

The binary mixture of the solvent is assumed to be in one-phase states away from the gas-liquid criticality. The electrostatic and amphiphilic interactions are not treated explicitly. The boundary effect is beyond the scope of this paper. In all the calculations to follow, we fix the temperature T at 300 K, so we do not write the T -dependence of the physical quantities.

A. Solvation chemical potential

The Helmholtz free energy density $f(n_1, n_2, n_3)$ is expanded with respect to n_3 up to second order as^{36,37}

$$f = f_m + k_B T [\ln(n_3 \lambda_3^3) - 1 + \nu_3] n_3 + \frac{1}{2} U_{33} n_3^2, \quad (2)$$

where $f_m(n_1, n_2)$ is the solvent free energy density and $\lambda_3 (\propto T^{-1/2})$ is the solute thermal de Broglie length. The $k_B T \nu_3(n_1, n_2)$ is the solvation chemical potential for a solute particle, which arises from the interactions with its surrounding solvent. The last term represents the (direct) solute-solute interaction defined by

$$U_{33} = \lim_{n_3 \rightarrow 0} [(\partial \mu_3 / \partial n_3)_{T, n_1, n_2} - k_B T / n_3], \quad (3)$$

where n_1 and n_2 are fixed and the ideal gas part ($\propto n_3^{-1}$) is subtracted. The chemical potentials $\mu_i = \partial f / \partial n_i$ and the pressure $p = \sum_j n_j \mu_j - f$ are expanded up to first order corrections as

$$\mu_i = \mu_{mi} + k_B T \nu_{3i} n_3 \quad (i = 1, 2), \quad (4)$$

$$\mu_3 = k_B T [\ln(n_3 \lambda_3^3) + \nu_3] + U_{33} n_3, \quad (5)$$

$$p = p_m + k_B T (1 + \zeta_3) n_3. \quad (6)$$

Here, we define $\mu_{mi}(n_1, n_2) = \partial f_m / \partial n_i$ and $p_m(n_1, n_2) = \mu_{m1} n_1 + \mu_{m2} n_2 - f_m$. We also introduce

$$\nu_{31} = (\partial \nu_3 / \partial n_1)_{T, n_2}, \quad \nu_{32} = (\partial \nu_3 / \partial n_2)_{T, n_1}, \quad (7)$$

$$\zeta_3 = n_1 \nu_{31} + n_2 \nu_{32} = n (\partial \nu_3 / \partial n)_{T, X}, \quad (8)$$

where $n = n_1 + n_2$ is the solvent number density. In this paper, we treat nearly incompressible solvents with small compressibility κ_m such that the inequality $n k_B T \kappa_m \ll 1$ holds for any X . In terms of p_m , κ_m is expressed as

$$\kappa_m^{-1} = n (\partial p_m / \partial n)_{T, X}, \quad (9)$$

where T and X are fixed in the derivative. See Eq. (A3) in Appendix A for another definition of the compressibility in many-component fluids. For example, $\kappa_m = 4.5 \times 10^{-4} / \text{MPa} \sim 0.05 / n_r k_B T$ for ambient liquid water with density $n_r = 33 / \text{nm}^3$ at 300 K and 1 atm.

It is convenient to introduce the partial volumes^{46–48} v_i for the three species in the dilute limit $n_3 \rightarrow 0$. As will be shown in Appendix A, they are expressed as

$$v_i = \kappa_m(\partial p_m / \partial n_i) \quad (i = 1, 2), \quad (10)$$

$$v_3 = k_B T \kappa_m (1 + \zeta_3). \quad (11)$$

These volumes depend on T , p , and X . For not small solutes with $v_3 \gtrsim n^{-1}$, we find $\zeta_3 \cong v_3 / k_B T \kappa_m \gg 1$ in nearly incompressible fluids (see Fig.3(d)). To understand the physical meaning of v_i , let us prepare a reference solvent with $n_1 = n_{r1}$ and $n_2 = n_{r2}$. We then add a solute at a small density n_3 . If T and p are held fixed, Eq.(A4) in Appendix A gives

$$v_1(n_1 - n_{r1}) + v_2(n_2 - n_{r2}) + v_3 n_3 \cong 0, \quad (12)$$

which holds in linear order in n_3 . If T , n_1 , and n_2 are held fixed (in a fixed volume), the pressure increases by $v_3 n_3 / \kappa_m$ from Eq.(A4).

B. Kirkwood-Buff theory

We also introduce the Kirkwood-Buff integrals^{49–57},

$$G_{ij} = \int d\mathbf{r} [g_{ij}(r) - 1], \quad (13)$$

where $g_{ij}(r)$ are the radial distribution functions tending to 1 at large r . They are related to the density correlation functions $H_{ij}(r) = \langle \delta \hat{n}_i(\mathbf{r}) \delta \hat{n}_j(\mathbf{0}) \rangle$ as

$$H_{ij}(r) = n_i n_j [g_{ij}(r) - 1] + n_i \delta_{ij} \delta(\mathbf{r}). \quad (14)$$

Here, we write the microscopically defined number densities as $\hat{n}_i(\mathbf{r})$ and their deviations as $\delta \hat{n}_i(\mathbf{r}) = \hat{n}_i(\mathbf{r}) - n_i$ with caret to avoid confusion with the averages n_i . Then,

$$I_{ij} = \int d\mathbf{r} H_{ij}(r) = n_i n_j G_{ij} + n_i \delta_{ij}, \quad (15)$$

which are the long-wavelength limits of the structure factors $S_{ij}(q) = \int d\mathbf{r} \exp[i\mathbf{q} \cdot \mathbf{r}] H_{ij}(r)$. Hereafter, for any space-dependent variables $\hat{A}(\mathbf{r})$ and $\hat{B}(\mathbf{r})$, we write⁴⁵

$$\langle \hat{A} : \hat{B} \rangle \equiv \int d\mathbf{r} [\langle \hat{A}(\mathbf{r}) \hat{B}(\mathbf{0}) \rangle - \langle \hat{A} \rangle \langle \hat{B} \rangle], \quad (16)$$

Then, we have $I_{ij} = \langle \hat{n}_i : \hat{n}_j \rangle$.

The G_{ij} for the solvent species ($i, j = 1, 2$) smoothly tend to those without solute as $n_3 \rightarrow 0$. We assume that G_{i3} ($i = 1, 2, 3$) tend to well-defined dilute limits $G_{i3}^0 = \lim_{n_3 \rightarrow 0} G_{i3}$. From Eqs.(11) and (A12), we obtain

$$\zeta_3 = -(n_1 v_1 G_{13}^0 + n_2 v_2 G_{23}^0) / k_B T \kappa_m, \quad (17)$$

$$v_3 = k_B T \kappa_m - (n_1 v_1 G_{13}^0 + n_2 v_2 G_{23}^0). \quad (18)$$

C. Density fluctuations in binary mixtures

We here examine the fluctuations in binary solvents (with $n_3 = 0$). Using the deviations $\delta \hat{n}_1$ and $\delta \hat{n}_2$, we introduce microscopically fluctuating variables for the volume fraction and the concentration of the solvent by

$$\delta \hat{\phi}(\mathbf{r}) = v_1 \delta \hat{n}_1 + v_2 \delta \hat{n}_2, \quad (19)$$

$$\delta \hat{X}(\mathbf{r}) = n^{-2} (n_1 \delta \hat{n}_2 - n_2 \delta \hat{n}_1), \quad (20)$$

From results in Appendix A, we find

$$\langle \hat{\phi} : \hat{\phi} \rangle = k_B T \kappa_m, \quad \langle \hat{X} : \hat{X} \rangle = \chi, \quad \langle \hat{\phi} : \hat{X} \rangle = 0. \quad (21)$$

The last relation indicates *orthogonality* between $\delta \hat{\phi}$ and $\delta \hat{X}$. In terms of G_{ij} for the solvent, the compressibility κ_m and the concentration variance χ are written as

$$k_B T \kappa_m = v_1^2 n_1 + v_2^2 n_2 + \sum_{i,j=1,2} v_i n_i v_j n_j G_{ij} \quad (22)$$

$$\begin{aligned} \chi &= n_1 n_2 / n^3 + (n_1^2 n_2^2 / n^4) (G_{11} + G_{22} - 2G_{12}) \\ &= n^{-1} k_B T (\partial X / \partial \Delta)_{T,p}, \end{aligned} \quad (23)$$

where G_{ij} are those for $n_3 = 0$ and $\Delta = \mu_2 - \mu_1$. The second line of Eq.(23) follows from Eq.(A13)⁴⁵. Here, the matrix I_{ij} is diagonalized by the linear transformations in Eqs.(19) and (20), so its determinant is given by

$$I_{11} I_{22} - I_{12}^2 = n^4 k_B T \kappa_m \chi. \quad (24)$$

In nearly incompressible mixtures, the fluctuations of $\delta \hat{\phi}$ are small, but those of $\delta \hat{X}$ can grow due to molecular clustering^{58–61} or near the consolute criticality⁴⁵.

The scattering intensity is proportional to the structure factor $I(q) = \langle |\mathcal{A}_{\mathbf{q}}|^2 \rangle$ of a linear combination $\mathcal{A} = Z_1 \delta \hat{n}_1 + Z_2 \delta \hat{n}_2$, where Z_1 and Z_2 are constants. Here, $\mathcal{A} = (Z_1 n_1 + Z_2 n_2) \delta \hat{\phi} + (Z_2 v_1 - Z_1 v_2) n^2 \delta \hat{X}$, so Eq.(21) yields the long-wavelength limit^{51,62},

$$I(0) = (Z_1 n_1 + Z_2 n_2)^2 k_B T \kappa_m + (Z_2 v_1 - Z_1 v_2)^2 n^4 \chi. \quad (25)$$

In water-alcohol mixtures, the concentration fluctuations are enhanced on nanometer scales due to the hydrogen-bonding interaction, on which a number of scattering experiments^{63–66} and molecular dynamics simulations^{58–61} were performed. The combination $n(G_{11} + G_{22} - 2G_{12})$ in χ in Eq.(23) exhibits a maximum as a function of the alcohol fraction, which is about 5 for methanol⁵¹, 20 for ethanol^{50–52,65}, and 100 for TBA^{52,64} and 1-propanol^{52,66}, depending on the degree of hydrophobic association of alcohol molecules⁶¹.

For our model mixture to be explained in Sec.III, we display the mixture quantities in Fig.1 and the normalized solvation chemical potential ν_3 in Eq.(2) in Fig.2 at $T = 300$ K and $p = 1$ atm. The behaviors in Fig.1 resemble those observed in water-alcohol mixtures, though we do not account for the hydrogen bonding.

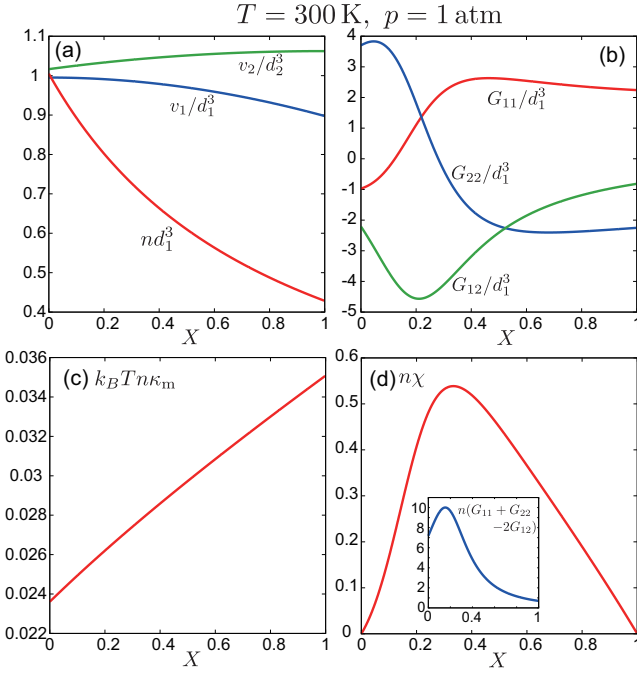


FIG. 1: Mixture behaviors without solute at $T = 300$ K and $p = 1$ atm from MCSL model, where $X = n_2/n$ is the cosolvent molar fraction with $n = n_1 + n_2$. Here, our mixture is in one-phase states due to a strong attractive interaction between the two species. The hard-sphere diameters are $d_1 = 3$ Å and $d_2 = 1.3d_1$. Thus, $d_1^3 = 0.0180$ L/mol and $d_1^{-3} = 55.6$ mol/L. Plotted are (a) partial volumes v_1 and v_2 divided by d_1^3 and density n multiplied by d_1^3 , (b) Kirkwood-Buff integrals G_{ij} divided by d_1^3 , (c) normalized compressibility $nk_B T \kappa_m (\ll 1)$, and (d) concentration variance χ in Eq.(23) multiplied by n . In (d), $n(G_{11} + G_{22} - 2G_{12})$ is also shown (inset), whose maximum is about 10 at $X \sim 0.2$. See Sec.III for details of our model.

D. Density fluctuations in ternary mixtures

In this subsection, we superimpose small density changes $\delta n_i(\mathbf{r})$ on the homogeneous averages n_i . These δn_i are coarse-grained variables slowly varying in space compared to the potential ranges. From Eq.(2) the second-order change in f is expressed as

$$\delta f_{\text{in}} = \frac{1}{2} k_B T \sum_{i,j=1,2,3} I^{ij} \delta n_i \delta n_j, \quad (26)$$

where $k_B T I^{ij} = \partial^2 f / \partial n_i \partial n_j = \partial \mu_i / \partial n_j = \partial \mu_j / \partial n_i$. The matrix $\{I^{ij}\}$ is equal to the inverse of the variance matrix $\{I_{ij}\}$ in Eq.(15). For small n_3 , Eq.(2) yields

$$I^{i3} = \nu_{3i} \quad (i = 1, 2), \quad I^{33} = 1/n_3 + U_{33}/k_B T. \quad (27)$$

Here, we neglect the n_3 -dependence of I^{ij} and I^{i3} ($i, j = 1, 2$) retaining the first diverging term ($\propto n_3^{-1}$) in I^{33} , which much simplifies the following calculations.

We introduce coarse-grained deviations of the volume

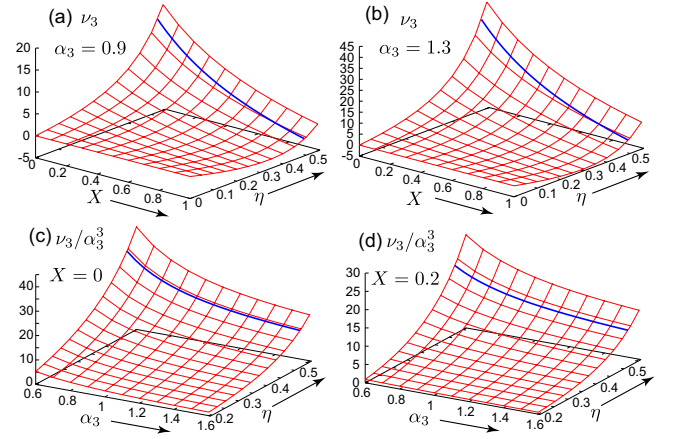


FIG. 2: Results of the normalized solvation chemical potential ν_3 in Eq.(2) for a hydrophobic solute with $\epsilon_{13} = 0$ and $\epsilon_{23}/k_B = 300$ K at $T = 300$ K from MCSL model. The solvation chemical potential is given by $k_B T \nu_3 = 2.48 \nu_3$ kJ/mol. The diameter ratio $\alpha_3 = d_3/d_1$ is (a) 0.9 and (b) 1.3 in the X - η plane, where $\eta = (\pi/6)(n_1 d_1^3 + n_2 d_2^3)$ is the hard-sphere volume fraction. Ratio ν_3/α_3^3 is displayed in the α_3 - η plane, where $X = n_2/(n_1 + n_2)$ is (c) 0 and (d) 0.2. For $\alpha_3 > 1$, ν_3 behaves as $\alpha_3^3 \propto \nu_3$. The solvent pressure p_m in Eq.(6) is 1 atm on blue curves. See Sec.III.

fraction and the concentration of the solvent by

$$\delta \phi = v_1 \delta n_1 + v_2 \delta n_2, \quad \delta X = n^{-2} (n_1 \delta n_2 - n_2 \delta n_1), \quad (28)$$

which are of the same forms as $\delta \hat{\phi}$ and $\delta \hat{X}$ in Eqs.(19) and (20). In terms of $\delta \phi$ and δX the solute-solvent coupling terms in $\delta f_{\text{in}}/k_B T$ are rewritten as

$$(I^{13} \delta n_1 + I^{23} \delta n_2) \delta n_3 = (\zeta_3 \delta \phi + g_3 \delta X) \delta n_3, \quad (29)$$

where ζ_3 is given in Eqs.(8) and (17). We define the solute-concentration coupling constant g_3 by^{53,67}

$$g_3 = n^2 (v_1 \nu_{32} - v_2 \nu_{31}) = (\partial \nu_3 / \partial X)_{T,p}. \quad (30)$$

At fixed T and p , Eqs.(A4) and (28) give $v_1 \delta n_1 + v_2 \delta n_2 = 0$ and $n^2 dX = v_1^{-1} \delta n_2 = -v_2^{-1} \delta n_1$, leading to Eq.(30). In terms of the Kirkwood-Buff integrals and the fluctuation variances, g_3 can also be expressed as

$$g_3 = -\frac{n_1 n_2}{n^2 \chi} (G_{23}^0 - G_{13}^0) = -\lim_{n_3 \rightarrow 0} \frac{\langle \hat{n}_3 : \hat{X} \rangle}{n_3 \langle \hat{X} : \hat{X} \rangle}, \quad (31)$$

with the aid of Eqs.(21) and (A12). The difference $G_{23}^0 - G_{13}^0 = k_B T n_2^{-1} (\partial \nu_3 / \partial \mu_2)_{T,p}$ represents the preferential adsorption of a cosolvent around a solute particle⁵⁶. Thus, $g_3 = (\partial \nu_3 / \partial X)_{T,p} < 0$ for hydrotropic cosolvents.

For nonvanishing ζ_3 and g_3 , $\delta f_{\text{in}}/k_B T$ is written as

$$\frac{\delta f_{\text{in}}}{k_B T} = \frac{(\delta \phi_{\text{tot}})^2}{2k_B T \kappa_m} + \frac{(\delta X + \chi g_3 \delta n_3)^2}{2\chi} + \frac{(\delta n_3)^2}{2I_{33}}. \quad (32)$$

In the first term, we define the deviation of the volume fraction including a small solute contribution as

$$\delta \phi_{\text{tot}} = v_1 \delta n_1 + v_2 \delta n_2 + v_3^{\text{in}} \delta n_3, \quad (33)$$

where we introduce a solute volume v_3^{in} by

$$v_3^{\text{in}} = k_B T \kappa_m \zeta_3 = v_3 - k_B T \kappa_m. \quad (34)$$

From Eq.(11) v_3^{in} is only slightly smaller than v_3 for small κ_m . The second term in Eq.(32) indicates that the solvent composition tends to change by $-\chi g \delta n_3$ with the doping. In the third term, I_{33} is the solute variance in Eq.(15). From Eq.(27) its inverse is expressed as

$$1/I_{33} = 1/n_3 + U_{33}^{\text{eff}}/k_B T. \quad (35)$$

The U_{33}^{eff} is the effective interaction parameter written as

$$\begin{aligned} U_{33}^{\text{eff}} &= U_{33} - k_B T \sum_{i,j=1,2} I_{ij} \nu_{3i} \nu_{3j} \\ &= U_{33} - (v_3^{\text{in}})^2 / \kappa_m - k_B T \chi g_3^2, \end{aligned} \quad (36)$$

where the second line follows from Eq.(32). The second term in the second line is also written as $-(k_B T)^2 \kappa_m \zeta_3^2$ in terms of ζ_3 . The last two terms are negative representing the solvent-mediated attractive interaction. Here, $I_{33}^{-1} = (\partial \mu_3 / \partial n_3)_{T, \mu_1, \mu_2}$ from Eq.(A7), so U_{33}^{eff} is defined as

$$U_{33}^{\text{eff}} = \lim_{n_3 \rightarrow 0} [(\partial \mu_3 / \partial n_3)_{T, \mu_1, \mu_2} - k_B T / n_3]. \quad (37)$$

which should be compared with U_{33} in Eq.(3).

In the second line of Eq.(36), the second term much exceeds $n^{-1} k_B T$ in magnitude for not small solutes in nearly incompressible solvents. This contribution is already known for one-component solvents⁶⁸⁻⁷⁴. In Sec.III, we shall see that the third term can even be larger than the second term. Thus, the right hand side of Eq.(35) vanishes when n_3 is equal to a spinodal density given by

$$n_3^{\text{spi}} = -k_B T / U_{33}^{\text{eff}}. \quad (38)$$

We then have $I_{33} = n_3 / (1 - n_3 / n_3^{\text{spi}})$ and

$$G_{33} = 1 / (n_3^{\text{spi}} - n_3), \quad (39)$$

at small nonvanishing n_3 . Its dilute limit is given by

$$G_{33}^0 = 1/n_3^{\text{spi}} = -U_{33}^{\text{eff}}/k_B T. \quad (40)$$

Here, $G_{33} > 0$ for $n_3 < n_3^{\text{spi}}$, while $G_{33} < 0$ for $n_3^{\text{spi}} < 0$. If $G_{33} > 0$, the interaction among the solute particles is attractive on the average, which can occur even if the direct interaction is repulsive ($U_{33} > 0$). With further increasing n_3 , we eventually encounter the unstable regime $n_3 > n_3^{\text{spi}} > 0$, leading to spinodal decomposition of gas-liquid or liquid-liquid phase transition⁴⁵. Similarly, Roij and Mulders⁷⁷ calculated demixing spinodal for binary hard-rod mixtures using the second virial expansion of the Helmholtz free energy density as in Eq.(26).

We also notice that the density fluctuations are enhanced as $n_3 \rightarrow n_3^{\text{spi}}$ in one-phase states. From Eq.(32), the concentration variance $\chi_R = \langle \hat{X} : \hat{X} \rangle$ increases as

$$\chi_R = \chi + g_3^2 \chi^2 n_3 / (1 - n_3 / n_3^{\text{spi}}), \quad (41)$$

where no phase-separated droplets are assumed and χ is defined in Eqs.(21) and (23). The second term can be significant compared to the background χ for $g_3^2 \chi n \gg 1$ even for small n_3 (see Fig.3(e) and Eq.(65)).

E. Space-filling condition

Because $v_3^{\text{in}} \cong v_3$ for small $\kappa_m \ll (nk_B T)^{-1}$, the combination $\delta \phi_{\text{tot}}$ in Eq.(33) represents the deviation of the total volume fraction from 1. The space integral of the first term in Eq.(32) yields the *steric free energy*,

$$F_{\text{steric}} = \int d\mathbf{r} \frac{1}{2\kappa_m} \left[\sum_{j=1,2,3} v_j \delta n_j \right]^2, \quad (42)$$

where δn_i can vary slowly in space. This free energy serves to realize the space-filling $\sum_j v_j n_j = 1$ even for inhomogeneous densities in the limit of small κ_m . See Eqs.(12) and (46) where this condition holds for homogeneous density changes. Previously, the steric free energy in the same form was assumed for polymer mixtures⁴⁵.

If the composition-dependence of v_i is weak at given T and p , the space-filling holds at any compositions with common v_i (depending on T and p). In our case, this is roughly the case in Fig.1(a) and Fig.3(b). It is worth noting that the Flory-Huggins theory for polymer mixtures and the Bragg-Williams theory of binary alloys^{44,45} are based on the space-filling *assumption*, where the volumes of constituent particles (monomers for polymers) are equal to the cell volume of an incompressible lattice.

F. Osmotic pressure

For mixture solvents, the osmotic pressure Π is the pressure difference $\Pi = p(n_1, n_2, n_3) - p(n_{r1}, n_{r2}, 0)$ at fixed chemical potentials $\mu_i(n_1, n_2, n_3) = \mu_i(n_{r1}, n_{r2}, 0)$ ($i = 1, 2$), where n_{r1} and n_{r2} are the solvent densities in a reference state with $n_3 = 0$. In the virial expansion $\Pi = k_B T (n_3 + B_2 n_3^2 + \dots)$, McMillan and Mayer⁷⁸ found the relation $B_2 = -G_{33}^0/2$ for one-component solvents. Large negative B_2 eventually leads to solute aggregation.

At fixed T , μ_1 , and μ_2 , we have $d\Pi = n_3 d\mu_3 = k_B T n_3 I_{33}^{-1} dn_3$ from Eq.(A8). Then,

$$\begin{aligned} \left(\frac{\partial \Pi}{\partial n_3} \right)_{T, \mu_1, \mu_2} &= k_B T / (1 + n_3 G_{33}) \\ &= k_B T (1 - n_3 / n_3^{\text{spi}}) \end{aligned} \quad (43)$$

where use is made of Eq.(39) in the second line. Thus,

$$B_2 = -1/2 n_3^{\text{spi}} = -G_{33}^0/2 = U_{33}^{\text{eff}}/2k_B T. \quad (44)$$

From Eq.(A8) we also find

$$\left(\frac{\partial n_i}{\partial n_3} \right)_{T, \mu_1, \mu_2} = \frac{n_i G_{i3}}{1 + n_3 G_{33}} \quad (i = 1, 2). \quad (45)$$

This is integrated to give $n_i - n_{r_i} \cong n_i G_{i3}^0 n_3$, for small n_3 at fixed T , μ_1 , and μ_2 . Therefore, from Eqs.(18) and (34), we find another form of the space-filling condition,

$$v_1(n_1 - n_{r1}) + v_2(n_2 - n_{r2}) + v_3^{\text{in}} n_3 \cong 0, \quad (46)$$

where v_3 in Eq.(12) is replaced by v_3^{in} .

For nonionic solutes in water, B_2 has been examined in experiments⁶⁸ and simulations^{69–74}. For charged colloidal particles in a mixture solvent, B_2 changed from positive to negative on approaching the consolute critical point before their near-critical aggregation^{75,76}.

G. Ostwald coefficient, Gibbs transfer free energy ΔG , and Henry's constant k_H

The solvation chemical potential $k_B T \nu_3$ is measurable in two-phase coexistence. Let phase α be a a solute-poor liquid and phase γ be a solute-rich gas or liquid. The densities are n_i^α in phase α and n_i^γ in phase γ ($i = 1, 2, 3$). The Ostwald coefficient is defined by $L = n_3^\alpha/n_3^\gamma$ for the solute in equilibrium. Its dilute limit is written as⁷⁹

$$L_0 = \lim_{n_3 \rightarrow 0} L = \exp[-(\Delta G)_3/k_B T], \quad (47)$$

where $(\Delta G)_3$ is the Gibbs transfer free energy (from γ to α phase) for a solute particle. Since μ_3 in Eq.(5) assumes the same value in the two phases, we find

$$(\Delta G)_3/k_B T = \nu_3(n_1^\alpha, n_2^\alpha) - \nu_3(n_1^\gamma, n_2^\gamma). \quad (48)$$

If the γ phase is a gas far below the criticality, we obtain $(\Delta G)_3/k_B T \cong \nu_3(n_1^\alpha, n_2^\alpha)$, since ν_3 is small in gas. For example, $\Delta G/k_B T \cong 3.4$ for O_2 in water at $T = 300$ K.

Henry's constant is defined in gas-liquid coexistence. Its usual definition is $k_H = f_3/x_3^\alpha$, where

$$f_3 = k_B T \lambda_3^{-3} \exp(\mu_3/k_B T) \cong k_B T n_3 e^{\nu_3} \quad (49)$$

is the solute fugacity and $x_3^\alpha = n_3^\alpha/\sum_j n_j^\alpha$ is the solute molar fraction in liquid⁸⁰. As $n_3 \rightarrow 0$ we have

$$k_H^0 = \lim_{n_3 \rightarrow 0} k_H = k_B T n_\ell \exp[\nu_3(n_1^\alpha, n_2^\alpha)], \quad (50)$$

where $n_\ell = n_1^\alpha + n_2^\alpha$ is the liquid density. Thus, $k_H^0 \cong k_B T n_\ell/L_0$ far from the criticality.

Tucker and Christian⁸⁰ furthermore obtained the correction $k_H/k_H^0 - 1 = -87x_3^\alpha$ at small x_3^α for benzene in water at 308 K, which is weakly hydrophilic with $L_0 = 3.6$. In Appendix B, $k_H/k_H^0 - 1$ will be calculated to linear order in n_3^α or n_3^γ for one-component solvents as

$$k_H/k_H^0 - 1 = (2B_2^\alpha + 1/n_1^\alpha - 2v_3^\alpha)n_3^\alpha + k_B T \kappa_\alpha n_3^\alpha + v_3^\alpha(n_1^\alpha - n_1^\gamma)^{-1}(n_1^\alpha n_3^\gamma - n_1^\gamma n_3^\alpha), \quad (51)$$

where κ_α , v_3^α , and B_2^α are the liquid values of κ , v_3 , and B_2 . For benzene, we have $n_\ell B_2^\alpha \sim -50$ and $n_\ell v_3^\alpha \sim 10$, so the first term is dominant in Eq.(51) and can well explain the observed correction⁸⁰, as was shown by Rossky and Friedman⁸¹. However, for hydrophobic solutes with

$L_0 \ll 1$, we have $k_H/k_H^0 - 1 \cong v_3^\alpha n_3^\gamma$. See Appendix B for the correction $L/L_0 - 1$ of the Ostwald coefficient.

III. NUMERICAL RESULTS ON SOLVATION

In the density functional theory^{82–84}, use has been made of the Carnahan-Starling (CS) model for pure fluids¹⁸ and the Mansoori-Carnahan-Starling-Leland (MCSL) model for mixtures¹⁷ (see Appendices C and D). These models provide the equation of state for hard spheres in agreement with simulations¹⁷. In our previous paper³⁷, we used the MCSL model for water-oxygen mixtures. In this paper, we use it for ternary mixtures.

A. MCSL model and van der Waals model

For the coarse-grained smooth densities n_i , we write the Helmholtz free energy density as

$$f = \sum_{i=1,2,3} k_B T n_i [\ln(n_i \lambda_i^3) - 1] + f_h + f_a, \quad (52)$$

where f_h is the hard-sphere part and f_a is the attractive part. The potential from the boundary walls⁸² is not written. Each species has a hard-sphere diameter d_i . We write the diameter ratios as

$$\alpha_2 = d_2/d_1, \quad \alpha_3 = d_3/d_1. \quad (53)$$

In the literature^{82–84}, f_a has the pairwise form with Lennard-Jones potentials $\phi_{ij}(r)$ for $r > d_{ij} = (d_i + d_j)/2$. In this paper, we use the simple van der Waals form⁴⁵,

$$f_a = -\frac{1}{2} \sum_{i,j=1,2,3} w_{ij} n_i n_j. \quad (54)$$

The coefficients w_{ij} are related to the hard-sphere diameters and the Lennard-Jones energies ϵ_{ij} of ϕ_{ij} by^{83,84}

$$w_{ij} = - \int_{r>d_{ij}} dr \phi_{ij}(r) = \frac{4}{9} \sqrt{2} \pi \epsilon_{ij} (d_i + d_j)^3. \quad (55)$$

In our scheme, the chemical potentials are written as

$$\mu_i = k_B T \ln(n_i \lambda_i^3) + \mu_{hi} - \sum_j w_{ij} n_j, \quad (56)$$

See Eq.(D3) for the hard-sphere part $\mu_{hi} = \partial f_h / \partial n_i$.

As $n_3 \rightarrow 0$, we calculate ν_3 and U_{33} in Eq.(2) as

$$\nu_3(n_1, n_2) = [\lim_{n_3 \rightarrow 0} \mu_{h3} - w_{13} n_1 - w_{23} n_2] / k_B T, \quad (57)$$

$$U_{33}(n_1, n_2) = \lim_{n_3 \rightarrow 0} (\partial \mu_{h3} / \partial n_3) - w_{33}. \quad (58)$$

Here, ν_3 and U_{33} are complicated functions of $\eta = \pi(n_1 d_1^3 + n_2 d_2^3)/6$, X , α_2 , and α_3 (see Appendix D). They increase steeply with increasing $\eta \gtrsim 0.5$ and behave as $\alpha_3^3 \propto v_3$ and $\alpha_3^6 \propto v_3^2$, respectively, for $\alpha_3 > 1$. In particular, for one-component solvents ($n_2 = 0$) we obtain⁸⁵

$$\nu_3(n_1, 0) = (3\alpha_3 + 6\alpha_3^2 - \alpha_3^3)u_1 + 3\alpha_3^2 u_1^2 + \alpha_3^3 u_1^2 (4 + 2u_1) - (\alpha_3 - 1)^2 (2\alpha_3 + 1) \ln(1 - \eta_1) - w_{13} n_1 / k_B T, \quad (59)$$

where $\eta_1 = (\pi d_1^3/6)n_1$ and $u_1 = \eta_1/(1 - \eta_1)$.

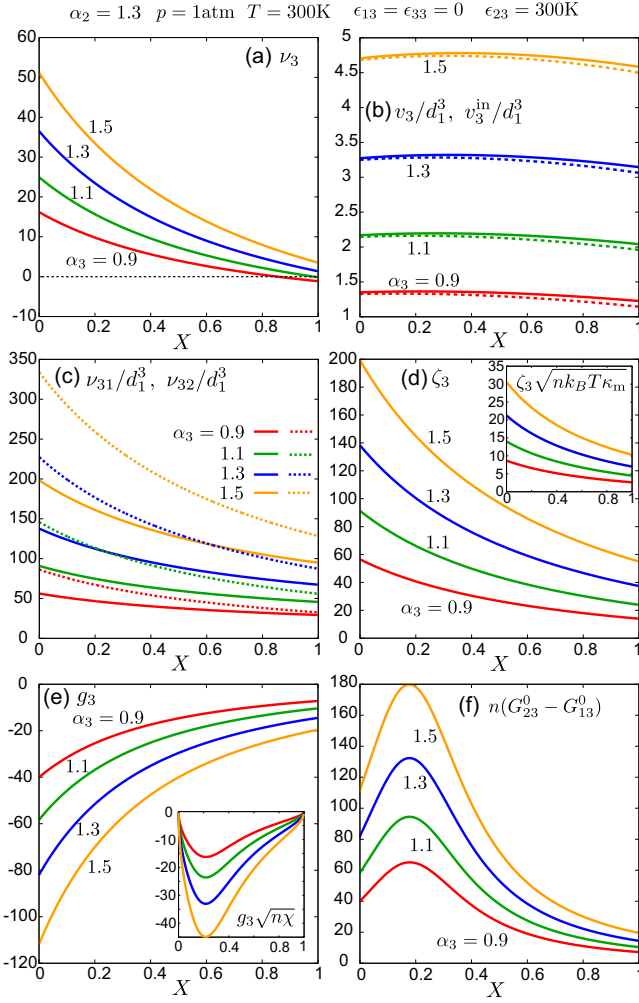


FIG. 3: Solvation quantities vs the cosolvent molar fraction X for a solute with diameter ratio $\alpha_3 = d_3/d_1 = 0.9, 1.1, 1.3,$ and 1.5 at $T = 300$ K and $p = 1$ atm, where the solvent is characterized by Eqs.(60) and (62) with $\epsilon_{13} = 0$ and $\epsilon_{23}/k_B = 300$ K. Plotted are (a) ν_3 , (b) solute partial volume v_3 (bold lines) and another volume v_3^{in} in Eq.(34) (dotted lines) divided by d_1^3 , which are very close, (c) density-derivatives ν_{31} (bold lines) and ν_{32} (dotted lines) in Eq.(7) divided by d_1^3 , (d) solute-density coupling coefficient ζ_3 in Eq.(8), (e) solute-concentration coupling coefficient g_3 in Eq.(30), and (f) degree of preferential adsorption $n(G_{23}^0 - G_{13}^0)$ appearing in Eq.(31). In insets in (d) and (e), $\chi_3(nk_B T \kappa_m)^{1/2}$ and $g_3(n\chi)^{1/2}$ are typical sizes of $\zeta_3 \delta \phi$ and $g_3 \delta X$ in Eq.(29).

B. Selected parameter values for mixture solvent

Supposing ambient water close to its gas-liquid coexistence as a reference state of the first species, we set

$$d_1 = 3 \text{ \AA}, \quad \epsilon_{11}/k_B = 588.76 \text{ K}, \quad (60)$$

where $w_{11}/\epsilon_{11}d_1^3 = 15.80$ from Eq.(55). We choose ϵ_{11} such that the coexistence (saturated vapor) pressure at $T = 300$ K is equal to its experimental one $p_{\text{cx}}^0 = 0.031$ atm (see Appendix C). The density in the reference state

n_r and the coexisting liquid and gas water densities, n_ℓ and n_g , at $T = 300$ K are calculated as

$$\begin{aligned} n_r &= 1.0049d_1^{-3}, & n_\ell &= n_r - 1.5 \times 10^{-5}n_r, \\ n_g &= p_{\text{cx}}^0/k_B T = 2.1 \times 10^{-5}n_r. \end{aligned} \quad (61)$$

The hard-sphere volume fraction is $\eta_1 = \pi n_r d_1^3/6 = 0.526$ for this n_r . The n_ℓ here is larger than the corresponding density of real water by 10 %. The compressibility is $1.71 \times 10^{-4}/\text{MPa} = 0.023/n_r k_B T$ in the reference state, while the experimental one is $4.5 \times 10^{-4}/\text{MPa}$.

We choose the parameters of the second species such that the mixture solvent remains in one-phase states at any X in ambient conditions. We thus set

$$d_2 = 3.9 \text{ \AA}, \quad \epsilon_{12}/k_B = 550 \text{ K}, \quad \epsilon_{22}/k_B = 500 \text{ K}, \quad (62)$$

for which $w_{12}/\epsilon_{11}d_1^3 = 22.44$ and $w_{22}/\epsilon_{11}d_1^3 = 29.47$. Here, ϵ_{12} and ϵ_{22} are close to ϵ_{11} . In Fig.1, we have displayed the mixture properties. We further make remarks. (i) As $n_2 \rightarrow 0$, the second species has the Gibbs transfer free energy $(\Delta G)_2 \cong -7.8k_B T$ at $T = 300$ K, so it is hydrophilic. (ii) At $T = 300$ K, the gas-liquid coexistence pressure p_{cx}^0 without solute is calculated as 0.031, 0.075, 0.089, 0.10, 0.11, and 0.13 in units of atm, where the molar fraction X^α of the second species in liquid is 0, 0.2, 0.4, 0.6, 0.8, and 1.0, respectively. These low pressures stem from the strong hydrophilicity of the second species (see Eq.(B3) and sentences below it). Note that the coexistence pressure of real water-alcohol mixtures is very low at room temperatures.

We then add a small amount of a hydrophobic solute. In most cases to follow, we set $\epsilon_{13} = \epsilon_{33} = 0$ and $\epsilon_{23} = 300$ K, for which the solute interacts with the two solvent species differently, resulting in a large solute-concentration coupling. In Fig.2, we have shown the overall behaviors of ν_3 in the X - η plane at fixed α_3 and ν_3/α_3^3 in the α_3 - η plane at fixed X . The ν_3 increases steeply with increasing η for $\eta \gtrsim 0.5$, decreases with increasing X , and behaves as α_3^3 for $\alpha_3 \gtrsim 1$ (see Appendix D for analytic results). The asymptotic relation $\nu_3 \sim \alpha_3^3$ is natural. The same result follows from the simple van der Waals model of fluid mixtures⁴⁵, where the steric free energy density is given by $-k_B T (\sum_i n_i) \ln(1 - \sum_i v_i^0 n_i)$, with v_i^0 being hard-sphere volumes.

In Fig.3, we plot quantities related to ν_3 vs X . Displayed are (a) ν_3 , (b) v_3 in Eq.(11) and v_3^{in} in Eq.(34), (c) ν_{31} and ν_{32} in Eq.(7), (d) ζ_3 in Eq.(8), (e) g_3 in Eq.(30), and (f) $n(G_{23}^0 - G_{13}^0)$. These quantities increase as α_3^3 with increasing α_3 . In the insets in (d) and (e), $\zeta_3(nk_B T \kappa_m)^{1/2}$ and $g_3(n\chi)^{1/2}$ indicate large sizes of $\zeta_3 \delta \phi$ and $g_3 \delta X$ in Eq.(29). In (d) and (e), the solute-solvent coupling coefficients ζ_3 and g_3 are both large. In (f), $n(G_{23}^0 - G_{13}^0)$ is peaked at $X \sim 0.2$. Previously, Booth *et al.*⁵⁶ found a maximum of $G_{23}^0 - G_{13}^0$ as a function of the hydrotrope density n_2 for various solutes (drugs) in water-hydrotrope mixture solvents.

We should have $|g_3| \gg 1$ and $g_3^2 n \chi \gg 1$ for relatively large hydrophobic solutes in water-hydrotrope solvents, especially in the presence of pre-Ouzo aggregates

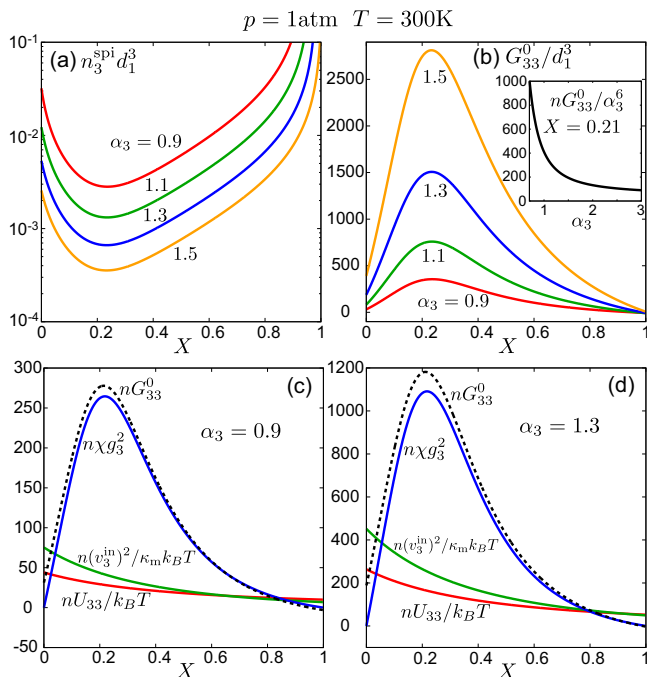


FIG. 4: Results as functions of the cosolvent molar fraction X for a solute with $\epsilon_{13} = \epsilon_{33} = 0$ and $\epsilon_{23}/k_B = 300$ K at $T = 300$ K and $p = 1$ atm. (a) Spinodal solute density $n_3^{\text{spi}} (= -k_B T/U_{33}^{\text{eff}})$ in Eq.(38) multiplied by d_1^3 and (b) Kirkwood-Buff integral $G_{33}^0 (= 1/n_3^{\text{spi}})$ in the dilute limit in Eq.(40) divided by d_1^3 , where the diameter ratio $\alpha_3 = d_3/d_1$ is 0.9, 1.1, 1.3, and 1.5. In inset in (b), nG_{33}^0/α_3^6 is plotted at $X = 0.21$. In (c) and (d), three contributions to $nU_{33}^{\text{eff}}/k_B T (= -nG_{33}^0)$ in Eq.(36) are compared for $\alpha_3 = 0.9$ and 1.3, respectively, where concentration contribution $n\chi g_3^2$ dominates and is nearly equal to nG_{33}^0 for $X \gtrsim 0.05$.

as thermal fluctuations^{8-11,14}. For water(1)-ethanol(2)-octanol(3), results of molecular dynamics simulation^{8,11} lead to rough estimations, $n(G_{13}^0 - G_{23}^0) = 100 - 300$, $-g_3 = 20 - 60$, and $g_3^2 n\chi = 300 - 3000$, at $X = 0.2$. For smaller (less hydrophobic) methane at $X \sim 0.2$, g_3 was numerically about -5 in water-methanol⁶⁷ and about -15 in water-TBA⁸⁶.

C. n_3^{spi} , G_{33}^0 , and B_2 for mixture solvent

The spinodal solute density n_3^{spi} , the Kirkwood-Buff integral G_{33}^0 , and the second osmotic virial coefficient B_2 are related as $G_{33}^0 = -2B_2 = 1/n_3^{\text{spi}}$ in Eqs.(40) and (44). In Fig.4, we plot (a) n_3^{spi} and (b) G_{33}^0 vs X , where the former (latter) decreases (increases) with increasing α_3 . The minimum of $n_3^{\text{spi}} d_1^3$ is small, which is 2.82×10^{-3} at $X = 0.236$ and is 6.63×10^{-4} at $X = 0.234$ for $\alpha_3 = 1.3$. In (c) and (d), we decompose $U_{33}^{\text{eff}}/k_B T (= -G_{33}^0)$ into $U_{33}/k_B T$, $-(v_3^{\text{in}})^2/k_B T \kappa_m$, and $-g_3^2 \chi$ from Eq.(36) and compare them for $\alpha_3 = 0.9$ and 1.3. For these examples, the concentration part dominates for not very small $X (\gtrsim 0.05)$ and the sum of the first two terms nearly vanishes

for $X \gtrsim 0.8$. Thus, for $g_3^2 n\chi \gg 1$ and $X \gtrsim 0.05$, we find

$$n_3^{\text{spi}} = 1/G_{33}^0 \cong (g_3^2 \chi)^{-1}. \quad (63)$$

D. n_3^{spi} , G_{33}^0 , and B_2 for one-component solvent

In nearly incompressible, one-component solvents ($X = 0$), there is no concentration part in Eq.(36), but the direct interaction U_{33} and the solvent-mediated one $-(v_3^{\text{in}})^2/\kappa_m$ are still large in magnitude ($\gg k_B T/n_1$) for not small solutes. They largely cancel but their difference can give large positive $G_{33}^0 = -2B_2$. The resultant attractive interaction leads to the well-known assembly of hydrophobic particles in ambient water³⁸⁻⁴⁰. Furthermore, for $n_3 > n_3^{\text{spi}} = 1/G_{33}^0$, spinodal decomposition of gas-liquid phase transition occurs. Previously, these two contributions to U_{33}^{eff} (or to B_2) have been calculated separately for one-component solvents^{70,71}, but there has been no analysis of their dependences on the solute size and the solute-solvent attractive interaction.

In Fig.5, we plot n_3^{spi} , G_{33}^0 , G_{33}^0/α_3^6 , and $(v_3^{\text{in}})^2/\kappa_m U_{33}$ vs α_3 at $X = 0$, where ϵ_{13}/k_B is 0, 250, and 400 K. In these cases, n_3^{spi} rapidly decreases to very small values with increasing α_3 . From (c) its behaves as

$$n_3^{\text{spi}} = 1/G_{33}^0 \sim A_0 n_1 \alpha_3^{-6} \quad (X = 0), \quad (64)$$

where $A_0 = 10^{-1} - 10^{-2}$ for not large $\epsilon_{13} (< \epsilon_{11})$. See Appendix D for analytic results. We can also see that G_{33}^0 decreases with increasing ϵ_{13} , as it should be the case. In (c), it is negative in the range $\alpha_3 < 1.22$ for $\epsilon_{13}/k_B = 400$ K, while it is positive for any α_3 at $\epsilon_{13} = 0$ (hard-sphere solutes)⁷³. In (d), the ratio of the two contributions to U_{33}^{eff} tends to a constant for each ϵ_{13} .

IV. PHASE SEPARATION WITH A SOLUTE

We now examine gas-liquid and liquid-liquid coexistence induced by a hydrophobic solute in our mixture solvent characterized by Eqs.(60) and (62) at $T = 300$ K. We require that the chemical potentials μ_i and the pressure p assume common values in coexisting two phases, so we treat macroscopic phase separation. The resultant densities are written as n_i^α in the solute-poor liquid phase and n_i^γ in the solute-rich phase. The surface tension is included in Sec.IVE in discussions of nucleation.

A. Solute-induced gas-liquid phase separation

In our gas-liquid transition, the solute is squeezed out of the liquid, while n_1^γ and n_2^γ remain small. In Fig.6, we show the densities in gas-liquid coexistence by varying the molar fraction $X^\alpha = n_2^\alpha/(n_1^\alpha + n_2^\alpha)$ at fixed pressure $p = p_{\text{cx}} = 1$ atm with $\alpha_3 = 1.1$. Gas-liquid coexistence in ternary mixtures is uniquely determined for each given T , p , and X^α . For our parameter choice, $(\Delta G)_3/k_B T$ in Eq.(48) decreases with increasing X^α , which is 25.0 at $X^\alpha = 0$ and 12.3 at $X^\alpha = 0.3$ for $\alpha_3 = 1.1$ (16.19 at

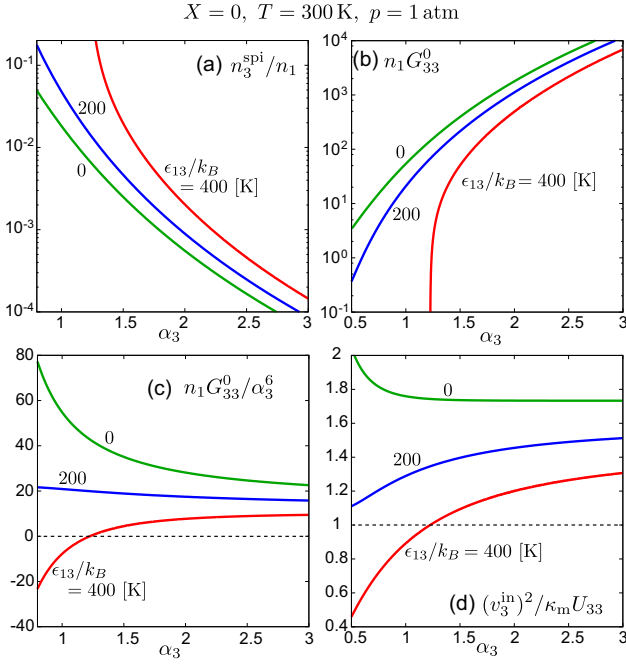


FIG. 5: Results in one-component solvent ($X = 0$) slightly outside the coexistence curve at $T = 300$ K and $p = 1$ atm. As functions of diameter ratio $\alpha_3 = d_3/d_1 (\leq 3)$, displayed are (a) spinodal solute density $n_3^{\text{spi}} (= -1/2B_2)$ divided by n_1 , (b) Kirkwood-Buff integral in the dilute limit $G_{33}^0 (= -2B_2)$ multiplied by n_1 , (c) $n_1 G_{33}^0 / \alpha_3^6$, and (d) $(v_3^{\text{in}})^2 / \kappa_m U_{33} = 1 - U_{33}^{\text{eff}} / U_{33}$ (see Eq.(36)). Here, ϵ_{12}/k_B takes three values (0, 250, and 400 K), which is 0 in the other figures in this paper. In (c), $G_{33}^0 \propto \alpha_3^6$ for large $\alpha_3 (\gtrsim 2)$ and G_{33}^0 changes its sign at $\alpha_3 = 1.22$ for $\epsilon_{12} = 400k_B$. In (d), the ratio tends to a constant larger than 1 with increasing α_3 , leading to $G_{33}^0 > 0$.

$X^\alpha = 0$ and 9.81 at $X^\alpha = 0.2$ for $\alpha_3 = 0.9$). The ratio n_2^0/n_2^γ stays close to its dilute limit ($n_2 \rightarrow 0$) given by $\exp(-(\Delta G)_2/k_B T) \sim e^8$. Thus, the second species plays the role of a cosolvent improving the solute solubility.

In Fig.7, we show that the pressure p_{cx} increases with increasing $n_3^\alpha = L_0 n_3^\gamma$ in gas-liquid coexistence fixed T and X^α . In (a), for the one-component solvent case, we plot p_{cx} vs n_3^α for $\alpha_3 = 0.9$ and 1.1. Also for $X^\alpha = 0.2$, we plot p_{cx} vs n_3^α for three values of α_3 at $\epsilon_{23}/k_B = 300$ K in (b) and for three values of ϵ_{23} at $\alpha_3 = 0.9$ in (c). For each n_3^α , p_{cx} largely increases with increasing the solute hydrophobicity. In (d), the ratio $(p_{\text{cx}} - p_{\text{cx}}^0)/k_B T n_3^\gamma$ tends to 1 for $n_3^\gamma d_1^3 \ll 1$ (see Eq.(65)), while it is between [1.1, 1.5] at $n_3^\gamma d_1^3 \sim 0.1$ due to the solute-solute repulsion. Larger n_3^γ can be obtained at higher pressures (up to $0.337d_1^{-3}$ in Fig.9(b)). Furthermore, if we include the attractive interaction among the solute particles ($\epsilon_{33} > 0$), n_3^γ can be increased up to a liquid density.

In the dilute limit $n_3^\gamma \ll d_1^{-3}$, p_{cx} is simply given by^{36,37}

$$p_{\text{cx}} - p_{\text{cx}}^0 = k_B T n_3^\gamma = k_B T L_0^{-1} n_3^\alpha = f_3 \quad (\text{GL}), \quad (65)$$

where p_{cx}^0 is the coexistence pressure without solute, L_0 is the Ostwald coefficient in Eq.(47), and f_3 is the solute

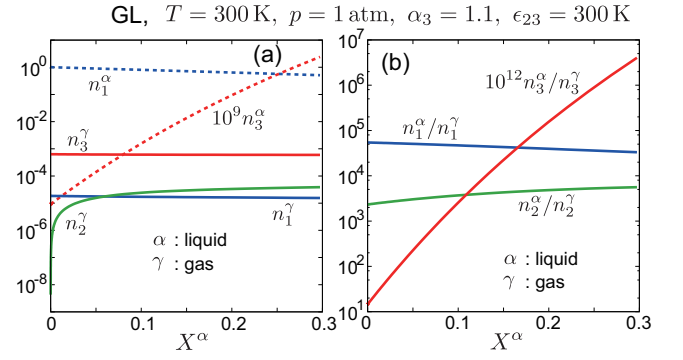


FIG. 6: Results of solute-induced gas-liquid coexistence at $T = 300$ K and $p = 1$ atm, where $\alpha_3 = 1.1$, $\epsilon_{13} = \epsilon_{33} = 0$, and $\epsilon_{23}/k_B = 300$ K. (a) Densities in liquid n_i^α (dotted lines) and those in gas n_i^γ (bold lines) in units of d_1^{-3} vs the cosolvent molar fraction in liquid $X^\alpha = n_2^\alpha / (n_1^\alpha + n_2^\alpha) (\leq 0.3)$, where the solute density in liquid n_3^α is extremely small. (b) Density ratios n_i^α/n_i^γ vs X^α , where those for the solvent ($i = 1, 2$) depend on X^α rather weakly but that for the solute (=the Ostwald coefficient L) depends on X^α very strongly.

fugacity in Eq.(49). In accord with Eq.(65), both L_0 and n_3^α increase with increasing X^α at fixed p_{cx} in Fig.6.

We can now discuss metastability of reference liquid states with respect to the gas-liquid transition by increasing its solute density \bar{n}_3 at given pressure $\bar{p} (> p_{\text{cx}}^0)$. In this isobaric condition, the solvent densities decrease according to Eq.(12). From Eq.(65), the liquid is stable for $\bar{n}_3 < n_3^b(\bar{p})$ but is metastable for $\bar{n}_3 > n_3^b$, where

$$n_3^b = L_0(\bar{p} - p_{\text{cx}}^0)/k_B T \quad (\text{GL}). \quad (66)$$

Recall that instability occurs for $\bar{n}_3 > n_3^{\text{spi}}$, where $n_3^{\text{spi}} (> n_3^b)$ is the spinodal solute density in Eq.(38). For very small L_0 and $\bar{p} - p_{\text{cx}}^0$, n_3^b can be extremely small. We may also change \bar{p} fixing \bar{n}_3 , where the liquid is metastable for $\bar{p} < p_b(\bar{n}_3)$. This p_b is the bubble-point pressure,

$$p_b = p_{\text{cx}}^0 + k_B T L_0^{-1} \bar{n}_3 \quad (\text{GL}), \quad (67)$$

which is equivalent to Eq.(65). For example, $p_b \sim 10^3$ atm if the solute molar fraction is of order L_0 . In pure water at $T \sim 300$ K, in contrast, bubble nucleation was observed for large negative pressures ($\sim -10^3$ atm)^{87,88}.

B. Phase transitions at fixed V - N_i - T

We also examine phase separation at fixed particle numbers N_i in a fixed volume V , where the initial one-phase state with densities $\bar{n}_i = N_i/V$ is metastable or unstable. For $\alpha_3 = 0.9$ and $\epsilon_{23}/k_B = 300$ K, we then encounter both gas-liquid and liquid-liquid phase transitions. The latter was also found for $\alpha_3 = 1.1$ and not for $\alpha_3 = 1.3$ if the other parameters were unchanged. This liquid-liquid phase separation occurs in a wider parameter region for larger ϵ_{23} , but disappears as $\epsilon_{23} \rightarrow 0$.

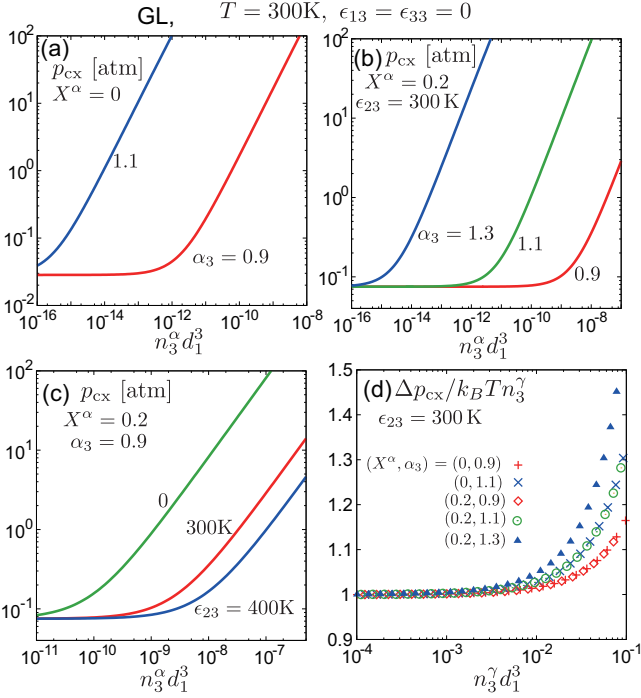


FIG. 7: Gas-liquid coexistence pressure p_{cx} in units of atm with addition of a hydrophobic solute with $\epsilon_{13} = \epsilon_{33} = 0$ at $T = 300$ K. As functions of $n_3^\alpha d_1^3$ on logarithmic scales, p_{cx} is plotted (a) for $X = 0$ with $\alpha_3 = 0.9$ and 1.1 , (b) for $X^\alpha = 0.2$ with $\alpha_3 = 0.9, 1.1$, and 1.3 at $\epsilon_{23}/k_B = 300$ K, and (c) for $X^\alpha = 0.2$ with $\epsilon_{23}/k_B = 0, 300$, and 400 K at $\alpha_3 = 0.9$. Here, $p_{cx} \rightarrow p_{cx}^0 (\ll 1 \text{ atm})$ as $n_3^\alpha \rightarrow 0$ (d) Ratio $\Delta p_{cx}/k_B T n_3^\gamma$ vs $n_3^\gamma d_1^3$ for five cases in (a) and (b) on a semi-logarithmic scale, where $\Delta p_{cx} = p_{cx} - p_{cx}^0$ is the pressure increase due to solute.

At fixed N_i and V , we consider the Helmholtz free energy. Its change after phase separation is written as

$$\mathcal{F} = V[\phi_\gamma f_\gamma + (1 - \phi_\gamma) f_\alpha - \bar{f}], \quad (68)$$

where ϕ_γ is the volume fraction of the γ phase, f_α and f_γ are the values of f in Eq.(52) in the two phases, and \bar{f} is the initial value of f . We seek minima of \mathcal{F} imposing the conditions $(1 - \phi_\gamma)n_i^\alpha + \phi_\gamma n_i^\gamma = \bar{n}_i$ ($i = 1, 2, 3$). To this end, we change $\phi_\gamma \rightarrow \phi_\gamma + \delta\phi_\gamma$ and $n_i^\gamma \rightarrow n_i^\gamma + \delta n_i^\gamma$ infinitesimally to obtain the incremental change in \mathcal{F} as

$$\delta\mathcal{F} = \sum_i (\mu_i^\alpha - \mu_i^\gamma) \delta N_i^\gamma + V(p_\alpha - p_\gamma) \delta\phi_\gamma, \quad (69)$$

where (p_α, μ_i^α) and (p_γ, μ_i^γ) are the values of (p, μ_i) in the two phases and $N_i^\gamma = V\phi_\gamma n_i^\gamma$ are the particle numbers in the γ phase. Thus, from $\partial\mathcal{F}/\partial\phi_\gamma = \partial\mathcal{F}/\partial n_i^\gamma = 0$, we obtain common values of p and μ_i in the two phases.

Figure 8 displays p_{cx} vs $\bar{x}_3 = N_3/(N_1 + N_2)$ at $\bar{X} = N_2/(N_1 + N_2) = 0.2$ in the two phase transitions. We set $\bar{n}_1 = N_1/V$ equal to (a) $0.6416d_1^{-3}$ and (b) $0.6327d_1^{-3}$, for which the initial pressure $\bar{p}_0 = p(\bar{n}_1, \bar{n}_2, 0)$ (without solute) is (a) 1 and (b) -613.5 atm. In (a), at $\bar{x}_3 = 10^{-4}$, p_{cx} is still 90 atm due to the presence of a gas

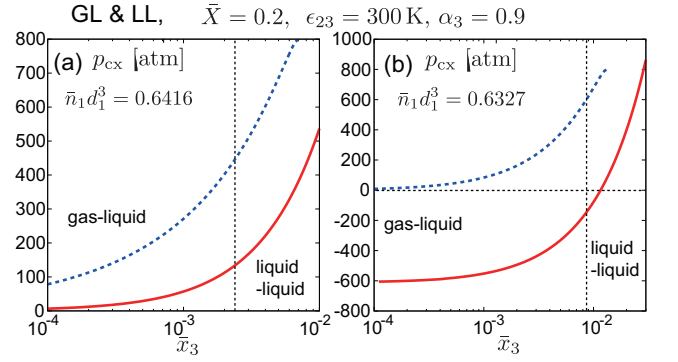


FIG. 8: Coexistence pressure p_{cx} vs average solute fraction $\bar{x}_3 = N_3/(N_1 + N_2)$ at fixed particle numbers $N_i = \bar{n}_i V$ in a fixed volume V , where gas-liquid (blue dotted lines) and liquid-liquid (red bold lines) transitions occur. Here, $\bar{n}_1 d_1^3$ is (a) 0.6416 and (b) 0.6327 , where $\bar{X} = N_2/(N_1 + N_2) = 0.2$, $\alpha_3 = 0.9$, $\epsilon_{13} = \epsilon_{33} = 0$, and $\epsilon_{23}/k_B = 300$ K. On the liquid-liquid branch, p_{cx} approaches (a) $p_{cx}^0 = 0.075$ atm and (b) -613.5 atm as $\bar{x}_3 \rightarrow 0$. On the gas-liquid branch, $p_{cx} - p_{cx}^0 \cong k_B T n_3^\gamma$ for $n_3^\gamma d_1^3 \ll 1$ as in Eq.(65).

fraction ($\sim 10^{-3}$ in Fig.9(c)) on the gas-liquid branch but is close to $\bar{p}_0 = 1$ atm on the liquid-liquid branch. In (b), as \bar{x}_3 is decreased, p_{cx} tends to $p_{cx}^0 = 0.075$ atm on the gas-liquid branch and to $\bar{p}_0 = -613.5$ atm on the liquid-liquid branch. Thus, in our model fluid, we can realize equilibrium liquid-liquid coexistence at negative pressures⁸⁹. Here, p_{cx} depends on n_3^α sensitively because ζ_3 in Eq.(6) is large (~ 40) in liquid as in Fig.2(c).

In Fig.9, we further show (a) n_i^α , (b) n_i^γ , (c) ϕ_γ , and (d) \mathcal{F} vs \bar{x}_3 for the case of Fig.8(a). The gas-liquid branch exists in the range $4 \times 10^{-8} < n_3^\gamma d_1^3 < 0.337$ here, on which the γ phase consists mostly of the solute. On the liquid-liquid branch, $n_2^\gamma d_1^3 (\sim 0.3)$ and $n_3^\gamma d_1^3 (\sim 0.2)$ are nearly constant (both increasing by 3% at $\bar{x}_3 = 10^{-2}$), while $n_1^\gamma d_1^3 (\sim 0.005)$ is small. In (c), ϕ_γ shrinks as $\bar{x}_3 \rightarrow 0$. In (d), \mathcal{F} is slightly lower (higher) on the gas-liquid branch than on the liquid-liquid branch in the left (right) of the vertical line at $\bar{x}_3 \sim 2.5 \times 10^{-3}$. However, from \mathcal{F} , we cannot decide which transition occurs in real situations.

To examine the metastability, we introduce the grand potential density $\omega(n_1, n_2, n_3)$ by^{36,45,93}

$$\omega = f - \sum_i \bar{\mu}_i n_i + \bar{p} = \sum_i (\mu_i - \bar{\mu}_i) n_i + \bar{p} - p, \quad (70)$$

where $\bar{\mu}_i$ and \bar{p} are the values of μ_i and p in the reference state with $n_i = \bar{n}_i$. Then, \mathcal{F} is rewritten as

$$\mathcal{F} = V[\phi_\gamma \omega_\gamma + (1 - \phi_\gamma) \omega_\alpha], \quad (71)$$

where ω_α and ω_γ are the values of ω in the two phases. Here, ω_α is of the second order in the deviations $n_i^\alpha - \bar{n}_i$ ($\propto \phi_\gamma$) as δf_{in} in Eq.(26), so $\omega_\alpha \propto \phi_\gamma^2$ as $\phi_\gamma \rightarrow 0$. On the other hand, we have $\omega_\gamma < 0$ when the initial state with $n_i = \bar{n}_i$ is metastable or unstable.

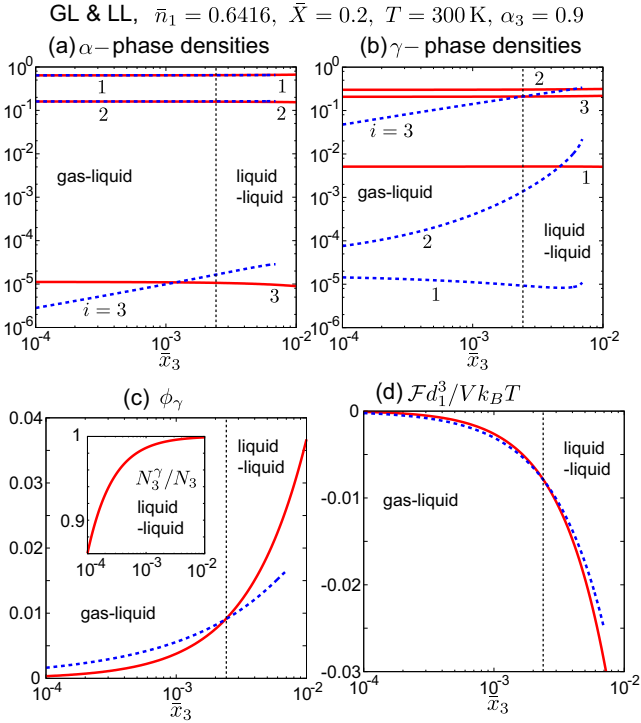


FIG. 9: Gas-liquid and liquid-liquid coexistence with varying $\bar{x}_3 = N_3/(N_1 + N_2)$ at $T = 300$ K, where particle numbers $N_i = \bar{n}_i V$ and volume V are fixed with $\bar{X} = N_2/(N_1 + N_2) = 0.2$ and $\bar{n}_1 d_1^3 = 0.6416$ as in Fig.8(a). Here, $\alpha_3 = 0.9$, $\epsilon_{13} = \epsilon_{33} = 0$, and $\epsilon_{23}/k_B = 300$ K. Plotted are (a) $n_i^\alpha d_1^3$ ($i = 1, 2, 3$) in the α phase on the gas-liquid branch (dotted lines) and on the liquid-liquid branch (bold lines), (b) $n_i^\gamma d_1^3$ in the γ phase, (c) volume fraction ϕ_γ of the γ phase, and (d) free energy change \mathcal{F} in Eq.(68) multiplied by $d_1^3/V k_B T$. In (c), solute number $N_3^\gamma = V \phi_\gamma n_3^\gamma$ in the γ phase divided by N_3 is also plotted (inset), which tends to 1 with increasing \bar{x}_3 . In (d), difference of \mathcal{F} between the two phases is very small.

In Fig.10, we plot ω_γ vs \bar{x}_3 at $\bar{X} = 0.2$ and 0.4 . For curves at fixed V we used the data in Figs.8(a) and 9, on which $\omega_\gamma < 0$. On the gas-liquid branch, $\omega_\gamma \rightarrow 0$ as $\phi_\gamma \rightarrow 0$, since $\bar{p}_0 = p(\bar{n}_1, \bar{n}_2, 0) = 1$ atm is close to p_{cx}^0 . The liquid-liquid branch exists only for $\bar{x}_3 > x_3^{\text{min}}$, where $\phi_\gamma \rightarrow 0$ and $\bar{n}_i \rightarrow n_i^\alpha$ as $\bar{x}_3 \rightarrow x_3^{\text{min}}$. In Fig.10, x_3^{min} is 1.41×10^{-5} at $\bar{X} = 0.2$ and 7.20×10^{-4} at $\bar{X} = 0.4$.

C. Phase transitions at fixed p - N_i - T

We next seek two-phase coexistence in the isobaric condition requiring $\mu_i^\alpha = \mu_i^\gamma$ and $p_\alpha = p_\gamma = 1$ atm. The average densities \bar{n}_i are chosen to satisfy $\bar{p} = p(\bar{n}_1, \bar{n}_2, \bar{n}_3) = 1$ atm. This is needed since $p_\alpha \rightarrow \bar{p}$ as $\phi_\gamma \rightarrow 0$. If we increase \bar{n}_3 gradually, \bar{n}_1 and \bar{n}_2 decrease according to Eq.(12) for each fixed $\bar{X} = \bar{n}_2/(\bar{n}_1 + \bar{n}_2)$. In this method, we vary the volumes of the two phases, V_α and V_γ , at fixed total particle numbers $N_i = \bar{n}_i \bar{V}$, where \bar{V} is the initial volume. Using ω in Eq.(70), we write the change

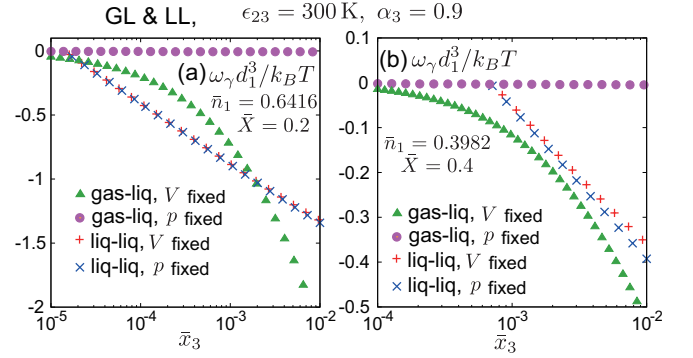


FIG. 10: Normalized grand potential density $\omega_\gamma d_1^3/k_B T$ in the γ phase vs $\bar{x}_3 = N_3/(N_1 + N_2)$ at $T = 300$ K, where $\bar{X} = N_2/(N_1 + N_2)$ is (a) 0.2 and (b) 0.4. On the gas-liquid branch, the pressure increases and ω_γ decreases with increasing \bar{x}_3 at fixed V (green filled triangle), while ω_γ is nearly zero at fixed p (purple filled circle). On the liquid-liquid branch, ω_γ is nearly the same for fixed V (red +) and p (blue \times). At fixed V in (a), the data are common to those in Fig.9. Here, $\alpha_3 = 0.9$, $\epsilon_{13} = \epsilon_{33} = 0$, and $\epsilon_{23}/k_B = 300$ K.

in the Gibbs free energy after phase separation as

$$\mathcal{G} = V_\alpha \omega_\alpha + V_\gamma \omega_\gamma. \quad (72)$$

The particle numbers $N_i^\alpha = V_\alpha n_i^\alpha$ and $N_i^\gamma = V_\gamma n_i^\gamma$ in the two phases satisfy $N_i^\alpha + N_i^\gamma = N_i$. For infinitesimal changes in these quantities, \mathcal{G} changes by

$$\delta \mathcal{G} = \sum_i (\mu_i^\gamma - \mu_i^\alpha) \delta N_i^\gamma + (\bar{p} - p_\alpha) \delta V_\alpha + (\bar{p} - p_\gamma) \delta V_\gamma. \quad (73)$$

Thus, from $\partial \mathcal{G} / \partial n_i^\gamma = \partial \mathcal{G} / \partial V_\gamma = \partial \mathcal{G} / \partial V_\alpha = 0$, we obtain $\mu_i^\alpha = \mu_i^\gamma$ and $p_\alpha = p_\gamma = \bar{p}$. On the gas-liquid branch, we have $V_\alpha \cong \bar{V}$. On the liquid-liquid branch, n_i^γ are nearly constant satisfying the space-filling relation in Eq.(12), which are slightly smaller than those at fixed V .

In Fig.10, we additionally plot curves of ω_γ vs \bar{x}_3 for $\bar{X} = 0.2$ and 0.4 at fixed p as well as those at fixed V . On the gas-liquid branch at fixed p , ω_γ nearly vanishes at any \bar{x}_3 , because n_3^γ remains small ($\sim 6 \times 10^{-4} d_1^{-3}$). On the liquid-liquid branch, the two curves of ω_γ at fixed V and p almost coincide and depend on \bar{x}_3 logarithmically. These are because n_3^γ is changed only by a small amount ($\lesssim 3\%$ in the figure) and the term $-\bar{\mu}_3 n_3^\gamma$ in ω_γ gives rise to the contribution $-k_B T n_3^\gamma \ln \bar{x}_3$ (see Eq.(80)).

D. Phase diagrams at fixed p - T

In Fig.11, the phase behaviors are illustrated for $\alpha_3 = 0.9$ at $T = 300$ K and $p = 1$ atm. In (a), stable and metastable regions of the liquid-liquid phase transition are separated by the binodal line $n_3^\alpha = n_3^{\text{min}}$ in the \bar{X} - n_3 plane. Here, n_3^{min} is the minimum of $\bar{n}_3 = \bar{x}_3(\bar{n}_1 + \bar{n}_2)$ on the isobaric liquid-liquid branch with $\bar{p} = p(\bar{n}_1, \bar{n}_2, \bar{n}_3) =$

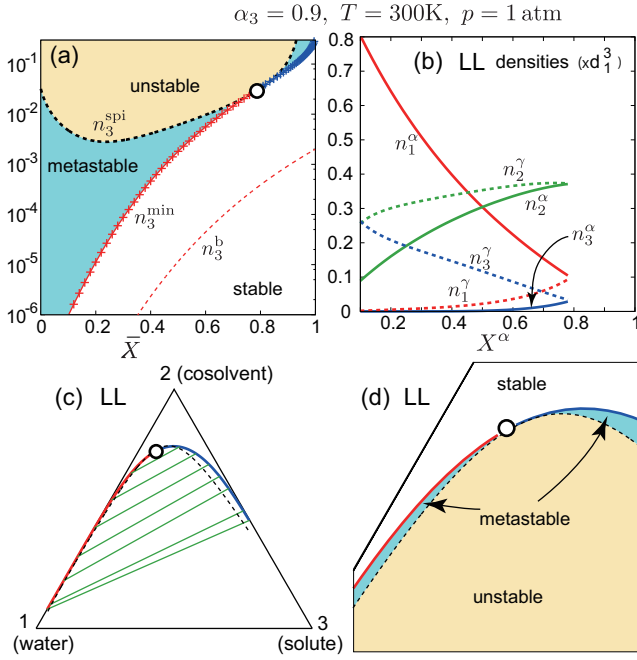


FIG. 11: Phase behaviors at $T = 300$ K and $p = 1$ atm for $\alpha_3 = 0.9$, $\epsilon_{13} = \epsilon_{33} = 0$, and $\epsilon_{23}/k_B = 300$ K. (a) Phase diagram in the \bar{X} - $n_3 d_1^3$ plane on a semi-logarithmic scale. Line n_3^{\min} vs \bar{X} separates stable and metastable (blue) regions of liquid-liquid transition, on which $\bar{X} = X^\alpha$. Unstable region is above line n_3^{spi} (yellow). Liquid-liquid critical point is marked by \circ . Binodal line is in red (blue) in the left (right) of the critical point. Liquid-liquid phase separation occurs above its binodal line n_3^{\min} (in blue and yellow). Line n_3^{b} represents bubble line at $p = 1$ atm for gas-liquid transition in Eq.(66). (b) Coexisting densities n_i^α and n_i^γ vs $X^\alpha = n_2^\alpha/(n_1^\alpha + n_2^\alpha)$ in units of d_1^{-3} , which coincide at the critical point. (c) Triangular phase diagram, where tie-lines (in green) connect coexisting two states. In (d), it is expanded near the critical point, where the metastable region (in green) is between the binodal and spinodal lines. In (a), (c), and (d), dotted lines represent spinodal.

1 atm (see Fig.10). At $\bar{n}_3 = n_3^{\min}$, we have $\phi_\gamma = 0$, $\bar{n}_i = n_i^\alpha$, and $\bar{X} = X^\alpha$ and obtain n_i^γ also. Above the spinodal line $\bar{n}_3 > n_3^{\text{spi}}$, the one-phase states are unstable against either of the two transitions. In (a), we also plot the bubble line $\bar{n}_3 = n_3^{\text{b}}$ ($\cong 0.8 \times 10^{-3} d_1^{-3} L_0$ here) in Eq.(66). On the other hand, in the region $n_3^{\text{b}} < \bar{n}_3 < n_3^{\text{spi}}$, the one-phase states are metastable with respect to the gas-liquid transition. In (b), we plot the densities n_i^α and n_i^γ vs X^α for the liquid-liquid transition, where we have $n_i^\alpha = n_i^\gamma$ at a critical point given by $X^\alpha = 0.78$ and $n_3^\alpha = 0.03 d_1^{-3}$ at fixed T and p . In (c) and (d), we present the triangular phase diagram of the liquid-liquid transition using the molar fractions x_i . For $x_2 \lesssim 0.7$, the binodal line is very close to the triangle boundaries for the present hydrophobic solute.

In liquid-liquid coexistence, the differential relation $\sum_i (n_i^\alpha - n_i^\gamma) d\mu_i^\alpha = 0$ holds, where μ_i^α are the α -

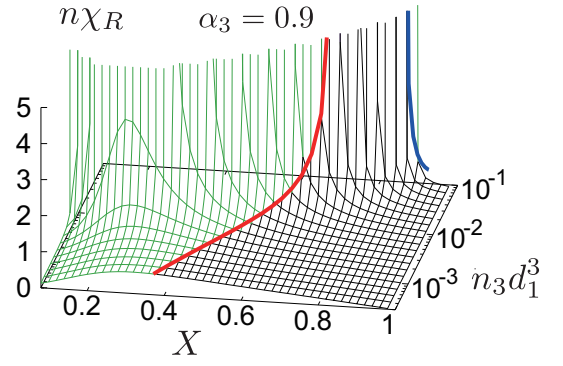


FIG. 12: Variance of the concentration fluctuations $n\chi_R$ ($n = n_1 + n_2$) in Eq.(41) in one-phase states at $T = 300$ K in the X - $n_3 d_1^3$ plane on a semi-logarithmic scale, where $\alpha_3 = 0.9$, $\epsilon_{13} = \epsilon_{33} = 0$, and $\epsilon_{23}/k_B = 300$ K. Contribution from phase-separated droplets is not included. It grows on approaching spinodal line and critical point (see Fig.11). Stable region (right) and metastable region (left) are separated by liquid-liquid binodal lines on the surface.

phase chemical potentials with $\mu_3^\alpha \cong k_B T [\ln(n_3^\alpha \lambda_3^3) + \nu_3(n_1^\alpha, n_2^\alpha)]$ from Eq.(5). We treat the binodal density $n_3^{\min} = n_3^\alpha$ as a function of X^α at fixed T and p to find

$$\left(\frac{\partial \ln n_3^{\min}}{\partial X^\alpha} \right)_{T,p} = -g_3 + \frac{n_2^\gamma n_1^\alpha - n_1^\gamma n_2^\alpha}{(n_3^\alpha - n_3^\gamma) n_2^\alpha \chi} \quad (\text{LL}), \quad (74)$$

using Eqs.(30) and (A13). Here, g_3 and χ are the α -phase values and $n_\alpha = n_1^\alpha + n_2^\alpha$. In Fig.11(a), the above derivative is close to $-g_3$, where the second term in Eq.(74) is about $0.1g_3$ and the critical value of g_3 is -10.4 .

In Fig.12, we plot the mean-field concentration variance χ_R in Eq.(41) in one-phase states in the stable and metastable regions, where $\alpha_3 = 0.9$, $T = 300$ K, and $p = 1$ atm. This χ_R does not include the contribution from phase-separated domains, but increases above χ due to the solute-concentration coupling in Eq.(29). We can approach the critical point in Fig.11 passing through the stable region with respect to the liquid-liquid transition to encounter the critical scattering.

Previously, Moriyoshi *et al.*⁹⁰ found a solute-induced critical point in a mixture of water, ethanol, and C8-alkanol. Recently, Anisimov's group¹⁵ measured the surface tension near a critical point in a mixture of water, TBA, and cyclohexane, where the correlation length increased up to 9.5 nm. Singular behaviors around such a unique critical point are of great interest.

Though constructing a theory of surfactant-free microemulsions is a future project, we make some comments. If the second species is amphiphilic, emulsification can occur in the metastable region $n_3^{\min} < \bar{n}_3 < n_3^{\text{spi}}$, while long-wavelength fluctuations grow up to macroscopic sizes in the unstable region $\bar{n}_3 > n_3^{\text{spi}}$. (i) To support this simple scenario, Vitale and Katz⁵ and Sitnikova *et al.*⁷ observed micrometer-sized Ouzo droplets in a narrow metastable region and macroscopic phase sep-

aration in an unstable region in the phase diagram for strongly hydrophobic solutes in water-ethanol solvents. This was displayed in a plane of the ethanol fraction and the logarithm of the solute fraction as in Fig.11(a). (ii) Anisimov's group^{13,14} observed droplets with sizes of order 100 nm in a narrow region in the triangular phase diagram at small cyclohexane fractions *outside the binodal* in a water-TBA solvent. They also observed mesoscopic droplets in wider regions outside the binodal for less hydrophobic solutes in the same solvent¹⁴. (iii) Through the Ouzo process, mesoscopic articles with sizes of order 100 nm can be produced for various hydrophobic solutes including polymers^{91,92} in water-hydrotrope mixtures.

E. Solute-induced nucleation

We now discuss homogeneous nucleation^{45,83,84,93,94} in a reference metastable state with densities \bar{n}_i and pressure \bar{p} . We suppose a spherical domain with radius R in the limit $\phi_\gamma \rightarrow 0$. The droplet free energy is given by

$$F(R) = (4\pi/3)R^3\omega_\gamma + 4\pi R^2\sigma, \quad (75)$$

where ω_γ is defined in Eq.(70) and the second term is the surface free energy. The surface tension σ is assumed to be a constant. This $F(R)$ depends on R , n_i^γ , and \bar{n}_i . For small changes in R and n_i^γ at fixed \bar{n}_i , $F(R)$ changes as

$$\frac{\delta F(R)}{4\pi R} = (R\omega_\gamma + 2\sigma)\delta R + \frac{R^2}{3} \sum_i (\mu_i^\gamma - \bar{\mu}_i) \delta n_i^\gamma. \quad (76)$$

We determine n_i^γ setting $\mu_i^\gamma = \bar{\mu}_i$ to seek a critical droplet. Then, Eq.(70) gives a simple relation,

$$\omega_\gamma = \bar{p} - p_\gamma < 0. \quad (77)$$

Since the second term in Eq.(76) vanishes, $F(R)$ has a maximum $F_c = F(R_c)$ at a critical radius R_c , where

$$R_c = 2\sigma/(p_\gamma - \bar{p}), \quad F_c = (4\pi/3)\sigma R_c^2. \quad (78)$$

These relations are general. In particular, we find $\omega_\gamma \cong (1 - n_1^\gamma/n_1^\alpha)(\bar{p} - p_{cx}^0)$ for weak metastability in one-component fluids^{45,94}, where the condition $\mu_1^\gamma = \bar{\mu}_1$ becomes $(p_\gamma - p_{cx}^0)/n_1^\gamma \cong (\bar{p} - p_{cx}^0)/n_1^\alpha$.

At the gas-liquid transition with $n_3^\gamma \ll d_1^{-3}$, we find $n_3^\gamma \cong L_0^{-1}\bar{n}_3$ from $\mu_3^\gamma = \bar{\mu}_3$, so use of p_b in Eq.(67) yields

$$\omega_\gamma \cong \bar{p} - p_b \quad (\text{GL}). \quad (79)$$

At the liquid-liquid transition, we use the relation $d\omega_\gamma \cong \sum_i (n_i^\alpha - n_i^\gamma) d\bar{\mu}_i = (n_3^\alpha - n_3^\gamma) d(\bar{\mu}_3 - \mu_3^{\min})$ with $\mu_3^{\min} = \mu_3(\bar{n}_1, \bar{n}_2, n_3^{\min})$. Here, $n_3^{\min}(\bar{n}_1, \bar{n}_2)$ is the binodal solute density for densities \bar{n}_1 and \bar{n}_2 . Thus,

$$\omega_\gamma \cong -k_B T (n_3^\gamma - n_3^\alpha) \ln(\bar{n}_3/n_3^{\min}) \quad (\text{LL}), \quad (80)$$

which is negative for $\bar{n}_3 > n_3^{\min}$. The curves of ω_γ at fixed p in Fig.10 can well be fitted to Eq.(80).

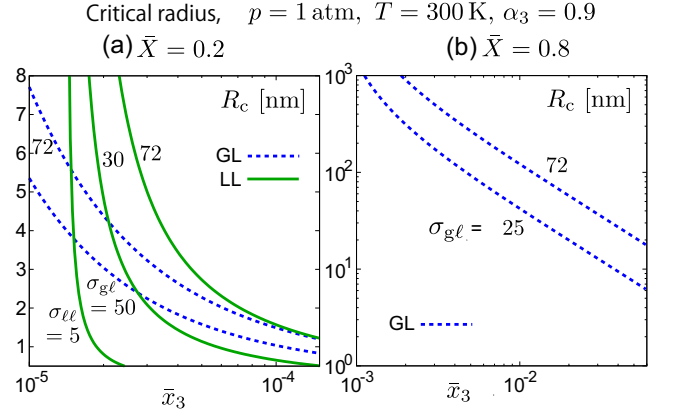


FIG. 13: Critical radius R_c for gas-liquid and liquid-liquid transitions vs $\bar{x}_3 = \bar{n}_3/(\bar{n}_1 + \bar{n}_2)$ in metastable states with densities \bar{n}_i at $T = 300$ K and $p = 1$ atm. Here, $\bar{X} = \bar{n}_2/(\bar{n}_1 + \bar{n}_2)$ is (a) 0.2 and (b) 0.8 with $\alpha_3 = 0.9$, $\epsilon_{13} = \epsilon_{33} = 0$, and $\epsilon_{23}/k_B = 300$ K. In units of mN/m, the gas-liquid surface tension σ_{gl} is (a) 72 and 50 and (b) 72 and 25, while the liquid-liquid surface tension σ_{ll} is 72, 30, and 5 in (a).

In our problem, we should note that σ depends on the composition X^α and take different values in gas-liquid and liquid-liquid phase transitions. Hence, we write $\sigma = \sigma_{gl}$ for the gas-liquid case and $\sigma = \sigma_{ll}$ for the liquid-liquid case. (i) For binary water-alcohol mixtures, σ_{gl} is decreased by interfacial adsorption of alcohol⁹⁵⁻⁹⁸. For example, at $X = 0.05$, it is 32 mN/m for ethanol and 25 mN/m for TBA, which are considerably below the pure-water value $\sigma_{gl}^w = 72$ mN/m. (ii) For ternary mixtures of water, alcohol, and a hydrophobic solute, σ_{ll} should be decreased more strongly since the oil side contains hydrophobic molecules⁹⁹. It was well below 1 mN/m as the critical pint was approached^{2,10,15}.

In Fig.13, we plot R_c in Eq.(77) vs \bar{x}_3 for (a) $\bar{X} = 0.2$ and (b) 0.8 in the metastable states in Fig.11(a), where $\alpha_3 = 0.9$, $T = 300$ K, and $p = 1$ atm. We write R_c for a few plausible values of σ_{gl} and σ_{ll} . In (a), R_c for the liquid-liquid transition is well below 1 nm with increasing \bar{x}_3 , where the nucleation barrier is negligible. In (b), R_c for the gas-liquid transition remains in the range $R_c \gtrsim 10$ nm even for $\sigma_{gl} = 25$ mN/m on approaching the critical point of the liquid-liquid transition, where homogeneous bubble nucleation is highly improbable. Note that bubble nucleation in pure water was detected when R_c was about 1 nm at large negative pressures at $T \sim 300$ K^{87,88}.

In water-alcohol solvents, nanometer-sized solute-rich aggregates preexist with alcohol molecules covering them in one-phase states^{8-11,13}. Then, they should play the role of *embryos* of critical liquid droplets consisting of solute and alcohol molecules. This much amplifies the prefactor I_0 of the nucleation rate $I = I_0 \exp(-F_c/k_B T)$ of the liquid-liquid transition^{45,94}. However, we can well expect occurrence of the gas-liquid transition for weak solute-cosolvent attraction (for smaller ϵ_{23} in our scheme) (see the first paragraph in Sec.IVB).

Jin *et al.*²⁵ reported observations of air nanobubbles in mixtures of water and a neutral organic water-soluble species such as tetrahydrofuran, where the latter has an amphiphilic nature and accumulates at gas-liquid interfaces. These bubbles were removed by repeated filtration and regenerated by air injection. Note that the method of gas injection is widely used to produce nanobubbles, where large bubbles are fragmented into small ones³¹.

V. SUMMARY AND REMARKS

We have studied a continuum theory of solvation and phase transitions in nonionic ternary mixtures varying the solvent composition X and the solute density n_3 . Main results are summarized as follows.

(1) In Sec.II, we have presented a theory of ternary mixtures using the second virial expansion of the free energy density f with respect to n_3 . We have clarified relationship among the solvation chemical potential $k_B T \nu_3$, the partial volumes v_i , the Kirkwood-Buff integrals G_{ij} (and the dilute limits G_{i3}^0), the solute spinodal density n_3^{spi} , the second virial osmotic coefficient B_2 , and the Gibbs transfer free energy ΔG . We have confirmed the space-filling relation $\sum_i v_i n_i = 1$ for slowly varying densities n_i in the limit of small compressibility. In nearly incompressible mixtures, the solute-concentration coupling grows as in Fig.4 when the solute interacts with the two solvent species differently. It is much amplified in water-alcohol mixtures in the presence of micelle-like aggregates^{8-11,13}.

(2) In Sec.III, we have investigated the solvation properties using the MCSL model. The parameters of our model have been chosen to realize the following at $T = 300$ K. (i) The saturated vapor pressure p_{cx}^0 is very small ($\ll 1$ atm), (ii) the two solvent species are miscible in any proportion at $p = 1$ atm, and (iii) the solute interacts repulsively with the first species but attractively with the second. In this situation, the solvent-mediated solute-solute interaction mainly arises from the solute-concentration coupling for not small X . In the case of one-component solvents ($X = 0$), we have examined the effective solute interaction vs the diameter ratio $\alpha_3 = d_3/d_1$ in Fig.5.

(3) In Sec.IV, we have examined solute-induced gas-liquid and liquid-liquid phase transitions. We have determined the solute spinodal density, the metastability conditions, and the binodal conditions. We have presented phase diagrams in Fig.11 and discussed homogeneous nucleation.

Finally, we give some remarks. (1) We need to calculate the surface tension for amphiphilic cosolvents. There should be significant differences between methanol, ethanol, and TBA in the formation of Ouzo domains. In the pre-Ouzo regime, the hydrotrope molecules consist of those forming micells and those in monomeric states^{9,16,57}. (2) Kinetics of solute-induced phase tran-

sitions should be investigated, where slow solute diffusion is crucial^{7,36,92}. (3) We can add a salt to water-hydrotrope mixtures^{28,66}. It is of interest how an antagonistic salt (composed of hydrophilic and hydrophobic ions) can induce aggregates in such mixture solvents¹⁰⁰, where an electric field can be applied¹⁰¹. (4) Microscopically, the hydrogen-bonding structures in aqueous mixtures are strongly deformed around amphiphilic and hydrophobic molecules. Thus, inputs from molecular dynamics simulations are highly informative^{8,11,13,59-61,67,86,99}.

Acknowledgments

We acknowledge support by JSPS KAKENHI Grant (No. JP18K03562 and No.15K05256). We would like to thank K. Koga and T. Sumi for informative discussions.

Appendix A: General relations of partial volumes and Kirkwood-Buff integrals

Let a nonionic fluid mixture be in a macroscopic volume V with particle numbers $N_i = n_i V$. The partial volumes, written as \bar{v}_i here, are defined by

$$\bar{v}_i = (\partial V / \partial N_i)_{T,p,\{N_{j \neq i}\}}, \quad (\text{A1})$$

where N_j with $j \neq i$ are fixed in the derivative with respect to N_i . We obtain $\bar{v}_i = (\partial \mu_i / \partial p)_{T,\{n_j\}}$ from $dG = -V dp + \sum_i \mu_i dN_i$ at fixed T for the Gibbs free energy G . Since V is an extensive quantity, we find the sum rule,

$$\sum_j \bar{v}_j n_j = 1. \quad (\text{A2})$$

The differential form of V is then given by

$$dV = \sum_j \bar{v}_j dN_j - \kappa V dp + \alpha_p V dT. \quad (\text{A3})$$

Here, $\kappa = -(\partial V / \partial p)_{T,\{N_j\}} / V$ is the isothermal compressibility and α_p is the isobaric thermal expansion coefficient. In Eq.(A3) we set $N_j = V n_j$ to obtain

$$\sum_j \bar{v}_j dn_j - \kappa dp + \alpha_p dT = 0, \quad (\text{A4})$$

with the aid of Eq.(A2). Thus, we can express \bar{v}_i as

$$\bar{v}_i = \kappa (\partial p / \partial n_i)_{T,\{n_{j \neq i}\}} \quad (\text{A5})$$

$$= k_B T \kappa \sum_j n_j I^{ij}. \quad (\text{A6})$$

In deriving Eq.(A6) we use the Gibbs-Duhem relation ($dp = \sum_j n_j d\mu_j$ at fixed T) and define

$$I^{ij} = (k_B T)^{-1} (\partial \mu_j / \partial n_i)_{T,\{n_{k \neq j}\}}. \quad (\text{A7})$$

We obtain Eqs.(10) and (11) from Eq.(A5).

In the grand canonical ensemble, we may consider the fluctuations of the particle numbers, written as $\delta\hat{N}_i$, in a region with volume V . The I_{ij} in Eq.(15) can be related to the variances of $\delta\hat{N}_i$ as

$$I_{ij} = V^{-1}\langle\delta\hat{N}_i\delta\hat{N}_j\rangle = k_B T(\partial n_i/\partial\mu_j)_{T,\{\mu_{k\neq j}\}}. \quad (\text{A8})$$

We notice that the matrix I^{ij} in Eq.(A7) is equal to the inverse of the variance matrix I_{ij} in Eq.(A8). Then,

$$k_B T \kappa n_i = \sum_j I_{ij} \bar{v}_j, \quad (\text{A9})$$

$$k_B T \kappa = \left[\sum_{jk} I^{jk} n_j n_k\right]^{-1} = \sum_{jk} I_{jk} \bar{v}_j \bar{v}_k. \quad (\text{A10})$$

It is easy to express I^{ij} in terms of I_{ij} for three component systems. Furthermore, for small n_3 , I_{ij} and I^{ij} for the solvent components ($i, j = 1, 2$) smoothly tend to those of $n_3 = 0$, while I^{33} grows as n_3^{-1} and

$$I^{i3} = -I^{i1}n_1G_{13} - I^{i2}n_2G_{23} + \dots \quad (i = 1, 2). \quad (\text{A11})$$

From Eqs.(4), (7), (A7), and (A11) we find

$$\begin{aligned} \nu_{3i} &= (k_B T)^{-1} \lim_{n_3 \rightarrow 0} (\partial\mu_i/\partial n_3)_{T, n_1, n_2} \\ &= - \lim_{n_3 \rightarrow 0} [I^{i1}n_1G_{13} + I^{i2}n_2G_{23}]. \end{aligned} \quad (\text{A12})$$

We then obtain Eqs.(17) and (31).

We finally consider the composition X for binary mixtures. Using Eqs.(A6) and (24), we rewrite its differential relation $dX = (n_1 dn_2 - n_2 dn_1)/n^2$ at fixed T as

$$\begin{aligned} dX &= (n^2 \chi/k_B T)(\bar{v}_1 d\mu_2 - \bar{v}_2 d\mu_1) \\ &= (n \chi/k_B T)[(\bar{v}_1 - \bar{v}_2) dp + d\Delta]. \end{aligned} \quad (\text{A13})$$

with $\Delta = \mu_2 - \mu_1$. For $dp = 0$ we find Eqs.(23) and (74).

Appendix B: Gas-liquid coexistence in one-component solvent: Corrections to L and k_H

In a one-component solvent, we examine gas-liquid coexistence with a solute to linear order in its density. The solvent and solute densities are n_1^α and n_3^α in liquid and n_1^γ and n_3^γ in gas. Without solute, the solvent density is n_ℓ in liquid and n_g in gas. After the doping, it is changed by $\delta n_1^\alpha = n_1^\alpha - n_\ell$ in liquid and $\delta n_1^\gamma = n_1^\gamma - n_g$ in gas.

The deviations $\delta\mu_1$, $\delta\mu_3$, and δp_{cx} assume common values in the two phases. The Gibbs-Duhem relation gives

$$\delta p_{\text{cx}} = n_\ell \delta\mu_1 + k_B T n_3^\alpha = n_g \delta\mu_1 + k_B T n_3^\gamma, \quad (\text{B1})$$

Here, for any physical quantity \mathcal{A} , we use the symbol $[\mathcal{A}] = \mathcal{A}_\alpha - \mathcal{A}_\gamma$, where the values of \mathcal{A} in the two phases are written with α and γ . We then solve Eq.(B1) as

$$\delta\mu_1/k_B T = -[n_3]/[n_1], \quad (\text{B2})$$

$$\begin{aligned} \delta p_{\text{cx}}/k_B T &= (n_1^\alpha n_3^\gamma - n_1^\gamma n_3^\alpha)/[n_1] \\ &= (n_\ell/L_0 - n_g)n_3^\alpha/(n_\ell - n_g) \end{aligned} \quad (\text{B3})$$

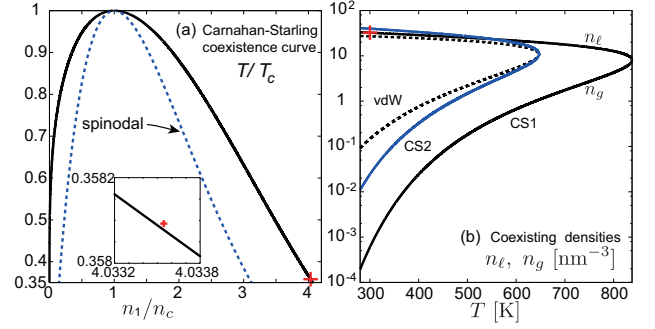


FIG. 14: Phase diagram of one-component solvent with Carnahan-Starling and van der Waals interactions. (a) Coexistence and spinodal curves in the T/T_c - n_1/n_c plane. Reference state in this paper is at $T = 300$ K slightly above the coexistence curve (red +) (see inset). (b) Coexisting liquid and gas densities n_ℓ and n_g vs T . On curve CS1 (bold line), use is made of Eq.(60), for which $p_{\text{cx}}^0 = 0.031$ atm at $T = 300$ K. Curves of CS2 (bold line) and vdW (dotted line) are obtained from the critical-point fitting.

Thus, δp_{cx} is positive (negative) for $L_0 n_g/n_\ell < 1$ (> 1). This occurs for $(\Delta G)_3/k_B T > -10.6$ (< -10.6) for ambient water. Far from the criticality, we have $\delta p_{\text{cx}} \cong k_B T n_3^\gamma$ for hydrophobic solutes as in Eq.(66), but the shift is small for hydrophilic solutes with $L_0 \gg 1$.

From Eq.(4) $\delta\mu_1$ is written as

$$\delta\mu_1/k_B T = \delta n_1^\alpha/K_\ell + \nu_\ell n_3^\alpha = \delta n_1^\gamma/K_g + \nu_g n_3^\gamma, \quad (\text{B4})$$

where (K_ℓ, ν_ℓ) and (K_g, ν_g) are the values of $K = n_1^2 k_B T \kappa$ and $\nu_{31} = \partial\nu_3/\partial n_1$ in liquid and gas, respectively, with κ being the compressibility. Here, Eq.(34) gives $K\nu_{31} = n_1 v_3^{\text{in}}$. From Eqs.(B2) and (B4) we find

$$\delta n_1^\alpha = -K_\ell([n_3]/[n_1] + \nu_\ell n_3^\alpha), \quad (\text{B5})$$

$$\delta n_1^\gamma = -K_g([n_3]/[n_1] + \nu_g n_3^\gamma), \quad (\text{B6})$$

In gas, $K_g \cong n_g$ and $\nu_g = \lim_{n_i \rightarrow 0} (\partial^2 p/\partial n_1 \partial n_3)$. Far from the criticality, δn_1^γ is very small ($\sim (n_g/n_\ell)n_3^\gamma$).

For the solute we use Eqs.(5) and (48) to obtain

$$[\ln n_3] + \Delta G/k_B T = -[\nu_{31} \delta n_1] - [U_{33} n_3]/k_B T, \quad (\text{B7})$$

where the left hand side is $\ln(L/L_0)$. With the aid of Eqs.(34) and (36), substitution of Eqs.(B5) and (B6) into the right hand side yields

$$L/L_0 - 1 = [n_1 v_3^{\text{in}}][n_3]/[n_1] - 2[B_2 n_3]. \quad (\text{B8})$$

The correction to k_H can be calculated from

$$\ln(k_H/k_H^0) = (\delta n_1^\alpha + n_3^\alpha)/n_\ell + \nu_\ell \delta n_1^\alpha + U_{33}^\alpha n_3^\alpha/k_B T, \quad (\text{B9})$$

where the quantities in liquid appear and the first term arises from $\ln[(n_1^\alpha + n_3^\alpha)/n_\ell]$. We thus find Eq.(51).

Appendix C: Phase diagram from CS model

For one-component fluids with density n_1 , Fig.14(a) displays a phase diagram, where the steric part is given by the Carnahan-Starling (CS) model and the attractive part by the van der Waals model¹⁰²⁻¹⁰⁴ with d_1 and w_{11} being independent of T and p . The pressure is given by

$$p = k_B T n_1 \left[1 + \frac{4\eta_1 - 2\eta_1^2}{(1 - \eta_1)^3} \right] - \frac{1}{2} w_{11} n_1^2, \quad (\text{C1})$$

where $\eta_1 = \pi d_1^3 n_1 / 6$. The critical temperature T_c , density n_c , and pressure p_c are calculated as^{103,104}

$$k_B T_c = 9.01 \times 10^{-2} w_{11} d_1^{-3}, \quad n_c = 0.249 d_1^{-3}, \\ p_c / n_c k_B T_c = 0.359. \quad (\text{C2})$$

In this paper, d_1 and w_{11} are given by Eq.(62), which yield the coexistence pressure $p_{\text{cx}}^0 = 0.031$ atm of water at $T = 300$ K (CS1 fitting). This gives $T_c = 838$ K and $n_c = 0.247 d_1^{-3} = 9.1 \text{ nm}^{-3}$, which are not far from the water values ($T_c = 647.1$ K and $n_c = 10.8 \text{ nm}^{-3}$). We can also determine d_1 and w_{11} to obtain T_c and n_c of water (CS2 fitting), for which $p_{\text{cx}}^0 = 0.72$ atm at $T = 300$ K. In Fig.14(b), curves CS1 and CS2 give the coexisting densities n_ℓ and n_g vs T from these fittings, which are compared with curve vdW from the critical-point fitting of the van der Waals model. In the CS model, the gas density $n_g (\cong p_{\text{cx}}^0 / k_B T)$ can be very small far below T_c .

Appendix D: Summary of MCSL model

We summarize the multi-component MCSL model¹⁷. Using d_i , we write the hard-sphere volume fractions as $\eta_i = \pi n_i d_i^3 / 6$ and the total one as $\eta = \sum_j \eta_j$. The hard-sphere free energy density f_h in Eq.(52) can be simply expressed in terms of $u = \eta / (1 - \eta)$ as

$$f_h / k_B T n = 4u + u^2 - 3y_1 u - 3(y_1 + y_2) u^2 / 2 \\ + (y_3 - 1)[u - u^2 / 2 - \ln(1 + u)], \quad (\text{D1})$$

where $n = \sum_j n_j$. We define y_1 , y_2 , and y_3 as

$$y_1 = \sum_{i>j} \frac{(d_i + d_j) \Delta_{ij}}{(d_i d_j)^{1/2}}, \quad y_2 = \frac{\xi_2}{\eta} \sum_{i>j} \Delta_{ij} (d_i d_j)^{1/2}, \\ y_3 = 6\xi_2^3 / \pi \eta^2 n, \quad (\text{D2})$$

where $\Delta_{ij} = (\pi/6)(d_i - d_j)^2 (d_i d_j)^{1/2} n_i n_j / n \eta$, and $\xi_\ell = (\pi/6) \sum_i n_i d_i^\ell$ ($\ell = 1, 2, 3$).

We then calculate the hard-sphere part of the chemical potential $\mu_{hi} = \partial f_h / \partial n_i$ in Eq.(56) as

$$\frac{\mu_{hi}}{k_B T} = (3\gamma_i^2 - 2\gamma_i^3 - 1) \ln(1 - \eta) + (2u^2 + 3u - 2) u \gamma_i^3 \\ + \frac{3\xi_2 d_i}{1 - \eta} \left(1 + \frac{\xi_1 d_i}{\xi_2} + \frac{\xi_0 d_i^2}{3\xi_2} + \frac{\xi_1 d_i^2 + \gamma_i}{1 - \eta} \right), \quad (\text{D3})$$

where $\gamma_i = \xi_2 d_i / \eta$. In ternary mixtures, μ_{h3} yields ν_3 and U_{33} as $n_3 \rightarrow 0$ from Eqs.(57) and (58). They have third-order and sixth-order polynomial forms as⁸⁵

$$\nu_3 = -\ln(1 - \eta) + D_1 \alpha_3 + D_2 \alpha_3^2 + D_3 \alpha_3^3, \quad (\text{D4})$$

$$n U_{33} = k_B T \sum_{0 \leq k \leq 6} W_k \alpha_3^k, \quad (\text{D5})$$

where the coefficients D_k and W_k depend on n_1 and n_2 . Note that n_3 appears in the form of $d_3^3 n_3$ in f_h in Eq.(D1), yielding the α_3^3 term in ν_3 and the α_3^6 term in U_{33} (see Figs.2 and 5). In particular, we express D_3 and W_6 as

$$D_3 = B^3 [2u^3 + u^2 - 2u - 2\ln(1 - \eta)] + 3A_1 B u^2 / A_3 \\ + u / A_3 - (8\sqrt{2}/3)(\epsilon_{13} \eta_1 + \epsilon_{23} \alpha_2^{-3} \eta_2) / k_B T, \quad (\text{D6})$$

$$W_6 = (B^3 / A_3) [5u^3 + 6u^2 - 6\ln(1 - \eta)] \\ + (1 + 6A_1 B u) u^2 / A_3, \quad (\text{D7})$$

where $A_\ell = 1 + X(\alpha_2^\ell - 1)$, $B = A_2 / A_3$, $\eta = \eta_1 + \eta_2$, and $u = \eta / (1 - \eta)$. The D_3 and W_6 are large for $\eta \gtrsim 0.5$. For example, we have $D_3 = 8.05 - 1.98\epsilon_{13} / k_B T$ for $X = 0$ and $\eta = 0.526$ and $D_3 = 6.00 - (1.27\epsilon_{13} + 0.317\epsilon_{23}) / k_B T$ for $X = 0.2$, $\eta = 0.520$, and $\alpha_3 = 0.9$. Thus, the coupling coefficients ζ_3 in Eq.(8) and g_3 in Eq.(30) increase as α_3^3 for $\alpha_3 \gtrsim 1$, leading to Eqs.(63) and (64).

¹ T. K. Hodgdon and E. W. Kaler, "Hydrotropic solutions," *Curr. Opin. Colloid Interface Sci.* **12**, 121-128 (2007).

² W. Kunz, K. Holmberg, and T. Zemb, "Hydrotropes," *Curr. Opin. Colloid Interface Sci.* **22**, 99-107 (2016).

³ K. J. Ruschak and C. A. Miller, "Spontaneous emulsification in ternary systems with mass transfer," *Ind. Eng. Chem. Fundam.* **11**, 534-540 (1972).

⁴ G. D. Smith, C.E. Donelan, and R. E. Barden, "Oil-continuous microemulsions composed of hexane, water, and 2-propanol," *J Colloid Interface Sci.* **60**, 488-496

(1977).

⁵ S. A. Vitale and J. L. Katz, "Liquid droplet dispersions formed by homogeneous liquid-liquid nucleation: the Ouzo effect," *Langmuir* **19**, 4105-4110 (2003).

⁶ I. Grillo, "Small-angle neutron scattering study of a world-wide known emulsion: Le Pastis," *Colloid. Surf. A: Physicochem. Eng. Aspects*, **225**, 153-160 (2003).

⁷ N. L. Sitnikov, R. Sprik, G. Wegdam, and E. Eiser, "Spontaneously formed *trans*-anethol/Water/alcohol emulsions: mechanism of formation and stability," *Langmuir* **21**,

- 7083-7089 (2005).
- ⁸ S. Schöttl, J. Marcus, O. Diat, D. Touraud, W. Kunz, T. Zemb, and D. Horinek, "Emergence of surfactant-free micelles from ternary solutions," *Chem Sci.* **5**, 2949-2954 (2014).
 - ⁹ P. Bošković, V. Sokol, T. Zemb, D. Touraud, and W. Kunz, "Weak micelle-like aggregation in ternary liquid mixtures as revealed by conductivity, surface tension, and light scattering," *J. Phys. Chem. B* **119**, 9933-9939 (2015).
 - ¹⁰ T. N. Zemb, M. Klossek, T. Lopian, J. Marcus, S. Schöttl, D. Horinek, S. F. Prevost, D. Touraud, O. Diat, S. Marčelja, and W. Kunz, "How to explain microemulsions formed by solvent mixtures without conventional surfactants," *PNAS* **113**, 4260-4265 (2016).
 - ¹¹ S. Schöttl and D. Horinek, "Aggregation in detergent-free ternary mixtures with microemulsion-like properties," *Curr. Opin. Colloid Interface Sci.* **22**, 8-13 (2016).
 - ¹² W. Hou and J. Xu, "Surfactant-free microemulsions," *Curr. Opin. Colloid Interface Sci.* **25**, 67-74 (2016).
 - ¹³ D. Subramanian, C. T. Boughter, J. B. Klauda, B. Ham-mouda, and M. A. Anisimov, "Mesoscale inhomogeneities in aqueous solutions of small amphiphilic molecules," *Faraday Discuss.* **167**, 217-238 (2013).
 - ¹⁴ D. Subramanian and M. A. Anisimov, "Phase behavior and mesoscale solubilization in aqueous solutions of hydrotropes," *Fluid Phase Equilibria* **362**, 170-176 (2014).
 - ¹⁵ A. A. Novikov, A. P. Semenov, V. Monje-Galvan, V. N. Kuryakov, J. B. Klauda, and M. A. Anisimov, "Dual action of hydrotropes at the water/oil interface," *J. Phys. Chem. C* **121**, 16423-16431 (2017).
 - ¹⁶ C. Tanford, "Theory of micelle formation in aqueous solutions," *J. Phys. Chem.* **78**, 2469-2479 (1974).
 - ¹⁷ G. A. Mansoori, N. F. Carnahan, K. E. Starling, T. W. Leland, "Equilibrium thermodynamic properties of the mixture of hard spheres," *J. Chem. Phys.* **54**, 1523-1525 (1971).
 - ¹⁸ N. F. Carnahan, K. E. Starling, "Equation of state for nonattracting rigid spheres," *J. Chem. Phys.* **51**, 635-636 (1969).
 - ¹⁹ G. W. Euliss and C. M. Sorensen, "Dynamic light scattering studies of concentration fluctuations in aqueous t-butyl alcohol solutions," *J. Chem. Phys.* **80**, 4767 (1984).
 - ²⁰ Y. Georgalis, A. M. Kierzek, and W. Saenger, "Cluster formation in aqueous electrolyte solutions observed by dynamic light scattering," *J. Phys. Chem. B* **104**, 3405 (2000).
 - ²¹ C. Yang, W. Li, and C. Wu, "Laser light-scattering study of solution dynamics of water/cycloether mixtures," *J. Phys. Chem. B* **108**, 11866 (2004).
 - ²² M. Sedláč, "Generation of multimacroion domains in polyelectrolyte solutions by change of ionic strength or pH ? macroion charge ?," *J. Chem. Phys.* **116**, 5256 (2002).
 - ²³ M. Sedláč, "Large-scale supramolecular structure in solutions of low molar mass compounds and mixtures of liquids: I. Light scattering characterization," *J. Phys. Chem. B* **110**, 4329 (2006).
 - ²⁴ C. Yang, W. Lei, C. Wu, "Laser light-scattering study of solution dynamics of water/cycloether mixtures," *J. Phys. Chem. B* **108**, 11866-11870 (2004).
 - ²⁵ F. Jin, J. Ye, L. Hong, H. Lam, and C. Wu, "Slow relaxation mode in mixtures of water and organic molecules: supramolecular structures or nanobubbles ?," *J. Phys. Chem. B* **111**, 2255 (2007).
 - ²⁶ M. Sedláč and D. Rak, "On the origin of mesoscale structures in aqueous solutions of tertiary butyl alcohol: the mystery resolved," *J. Phys. Chem. B*, **118**, 2726-2737 (2014).
 - ²⁷ A. E. Robertson, D. H. Phan, J. E. Macaluso, V. N. Kuryakov, E. V. Jouravleva, C. E. Bertrand, I. K. Yudin, M. A. Anisimov, "Mesoscale solubilization and critical phenomena in binary and quasi-binary solutions of hydro-trope," *Fluid Phase Equilibria* **407**, 243-254 (2016).
 - ²⁸ R. Okamoto and A. Onuki, "Precipitation in aqueous mixtures with addition of a strongly hydrophilic or hydrophobic solute," *Phys. Rev. E* **82**, 051501 (20 pp).
 - ²⁹ A. Onuki, R. Okamoto, and T. Araki, "Phase transitions in soft matter induced by selective solvation," *Bull. Chem. Soc. Jpn.* **84**, 569-587 (2011).
 - ³⁰ P. Attard, M. P. Moody, and J. W. G. Tyrrell, "Nanobubbles: the big picture," *Physica A* **314**, 696-705 (2002).
 - ³¹ K. Ohgaki, N. Q. Khanh, Y. Joden, A. Tsuji, and T. Nakagawa, "Physicochemical approach to nanobubble solutions," *Chem. Eng. Sci.* **65**, 1296-1300 (2010).
 - ³² T. Uchida, S. Oshita, M. Ohmori, T. Tsuno, K. Soejima, S. Shinozaki, Y. Take, and K. Mitsuda, "Transmission electron microscopic observations of nanobubbles and their capture of impurities in wastewater," *Nanoscale Research Lett.* **6**, 295 (9 pages) (2011).
 - ³³ J. R. T. Seddon and D. Lohse, "Nanobubbles and micropancakes: Gaseous domains on immersed substrates," *J. Phys.: Condens. Matter* **23**, 133001 (22 pp) (2011).
 - ³⁴ J. R. T. Seddon, D. Lohse, W. A. Ducker, V. S. J. Craig, "A deliberation on nanobubbles at surfaces and in bulk," *Chem. Phys. Chem.* **13**, 2179-2187 (2012).
 - ³⁵ D. Lohse and X. Zhang, "Surface nanobubbles and nanodroplets," *Rev. Mod. Phys.* **87**, 981 (2015).
 - ³⁶ R. Okamoto and A. Onuki, "Bubble formation in water with addition of a hydrophobic solute," *Eur. Phys. J. E* **38**, 72 (12 pp) (2015).
 - ³⁷ R. Okamoto and A. Onuki, "Density functional theory of gas-liquid phase separation in dilute binary mixtures," *J. Phys.: Condens. Matter* **28**, 244012 (16 pp) (2016).
 - ³⁸ B. Widom, P. Bhimalapuram, and K. Koga, "The hydrophobic effect," *Phys. Chem. Chem. Phys.* **5**, 3085-3093 (2003).
 - ³⁹ D. Chandler, "Interfaces and the driving force of hydrophobic assembly," *Nature* **437**, 640-647 (2005).
 - ⁴⁰ D. Ben-Amotz, "Water-mediated hydrophobic interactions," *Annu. Rev. Phys. Chem.* **67**, 617-638 (2016).
 - ⁴¹ T. M. Raschke, J. Tsai, and M. Levitt, "Quantification of the hydrophobic interaction by simulations of the aggregation of small hydrophobic solutes in water," *PNAS* **98**, 5965-5969 (2001).
 - ⁴² C. Oostenbrink and W. F. van Gunsteren, "Methane clustering in explicit water: effect of urea on hydrophobic interactions," *Phys. Chem. Chem. Phys.* **7**, 53-58 (2005).
 - ⁴³ L. Jiang, S. Cao, P. P. Cheung, X. Zheng, C. W. T. Leung, Q. Peng, Z. Shuai, B. Z. Tang, S. Yao, and X. Huang, "Real-time monitoring of hydrophobic aggregation reveals a critical role of cooperativity in hydrophobic effect," *Nat. Commun.* **8**, 15639 (8 pp) (2017).
 - ⁴⁴ P. J. Flory, *Principles of Polymer Chemistry* (Cornell Univ. Press, Ithaca, 1953), Chaps. 12 and 13.
 - ⁴⁵ A. Onuki, *Phase Transition Dynamics*; Cambridge University Press: Cambridge, U.K., 2002.
 - ⁴⁶ J. C. Moore, R. Battino, M. R. Rettlch, Y. P. Handa, and E. Willhelm, "Partial molar volumes of "gases" at infinite dilution in water at 298.15 K." *J. Chem. Eng. Data* **27**,

- 24-25 (1982).
- ⁴⁷ D. R. Biggerstaff and R. H. Wood, "Apparent molar volumes of aqueous argon, ethylene, and xenon from 300 to 716 K," *J. Phys. Chem.* **92**, 1988-1994 (1988).
- ⁴⁸ A. V. Plyasunov, E. L. Shock, J. P. O'Connell, "Corresponding-states correlations for estimating partial molar volumes of nonelectrolytes at infinite dilution in water over extended temperature and pressure ranges," *Fluid Phase Equilibria* **247**, 18-31 (2006).
- ⁴⁹ J. G. Kirkwood and F. P. Buff, "The statistical mechanical theory of solutions. I.," *J. Chem. Phys.* **19**, 774-777 (1951).
- ⁵⁰ A. Ben-Naim, "Inversion of the Kirkwood-Buff theory of solutions: Application to the water-ethanol system," *J. Chem. Phys.* **67**, 4884-4890 (1977).
- ⁵¹ M. C. A. Donkersloot, "The structure of binary liquids. The Kirkwood-Buff theory of liquid mixtures, illustrated on the basis of the systems water/methanol, water/ethanol, and cyclohexane/2,3-dimethylbutane, as a link between thermodynamic data and X-ray and neutron scattering results," *J. Solution Chem.* **8**, 293-307 (1979).
- ⁵² E. Matteoli and L. Lepori, "Solute-solute interactions in water. II. An analysis through the Kirkwood-Buff integrals for 14 organic solutes," *J. Chem. Phys.* **80**, 2856-2863 (1984).
- ⁵³ A. Ben-Naim, "Theory of preferential solvation of nonelectrolytes," *Cell Biophysics* **12**, 255-269 (1988).
- ⁵⁴ I. Shulgin and E. Ruckenstein, "Kirkwood-Buff integrals in aqueous alcohol systems: Comparison between thermodynamic calculations and X-ray scattering experiments," *J. Phys. Chem. B* **103**, 2496-2503 (1999).
- ⁵⁵ V. Pierce, M. Kang, M. Aburi, S. Weerasinghe, and P. E. Smith, "Recent applications of Kirkwood-Buff theory to biological systems," *Cell Biochem. Biophys.* **50**, 1-22 (2008).
- ⁵⁶ J. J. Booth, M. Omar, S. Abbott, and S. Shimizu, "Hydrotrope accumulation around the drug: the driving force for solubilization and minimum hydrotrope concentration for nicotinamide and urea," *Phys.Chem.Chem.Phys.* **17**, 8028-8037 (2015).
- ⁵⁷ S. Shimizu and N. Matubayasi, "Hydrotropy: monomeric equilibrium and minimum hydrotrope concentration," *J. Phys. Chem. B* **118**, 10515-10524 (2014).
- ⁵⁸ S. Dixit, J. Crain, W. Poon, J. Finney, and A. Soper, "Molecular segregation observed in a concentrated alcohol-water solution," *Nature* **416**, 829 (2002).
- ⁵⁹ L. Dougan, S. P. Bates, R. Hargreaves, J. P. Fox, J. Crain, and J. L. Finney, V. Réat, and A. K. Soper, "Methanol-water solutions: A bi-percolating liquid mixture," *J. Chem. Phys.* **121**, 6456-6462 (2004).
- ⁶⁰ R. Gupta and G. N. Patey, "Aggregation in dilute aqueous tert-butyl alcohol solutions: Insights from large-scale simulations," *J. Chem. Phys.* **137**, 034509 (12 pages) (2012).
- ⁶¹ S. Banerjee and B. Bagchi, "Stability of fluctuating and transient aggregates of amphiphilic solutes in aqueous binary mixtures: Studies of dimethylsulfoxide, ethanol, and tert-butyl alcohol," *J. Chem. Phys.* **139**, 164301 (2013).
- ⁶² A. B. Bhatia and D. E. Thornton, "Structural aspects of the electrical resistivity of binary alloys," *Phys. Rev.* **2**, 3004-3012 (1970).
- ⁶³ Y. Koga, "A SAXS study of concentration fluctuations in *t*-butanol-water system," *Chem. Phys. Lett.* **26**, 176-180 (1984).
- ⁶⁴ K. Nishikawa, Y. Kodera, and T. Iijima, "Fluctuations in the particle number and concentration and the Kirkwood-Buff parameters of *tert*-butyl alcohol and water mixtures studied by small-angle X-ray scattering," *J. Phys. Chem.* **91**, 3694-3699 (1987).
- ⁶⁵ K. Nishikawa and T. Iijima, "Small-angle X-ray scattering study of fluctuations in ethanol and water mixtures," *J. Phys. Chem.* **97**, 10824-10828 (1993).
- ⁶⁶ M. Misawa and K. Yoshida, "Concentration fluctuation and salt-induced percolation in 1-propanol aqueous solution," *J. Phys. Soc. Jap.* **69**, 3308-3314 (2000).
- ⁶⁷ K. Mochizuki and K. Koga, "Cononsolvency behavior of hydrophobes in water+methanol mixtures," *Phys. Chem. Chem. Phys.* **18**, 16188-16195 (2016).
- ⁶⁸ H. Liu and E. Ruckenstein, "Aggregation of hydrocarbons in dilute aqueous solutions," *J. Phys. Chem. B* **102**, 1005-1012 (1998).
- ⁶⁹ B. Widom and R. C. Underwood, "Second osmotic virial coefficient from the two-component van der Waals equation of state," *J. Phys. Chem. B* **116**, 9492-9499 (2012).
- ⁷⁰ K. Koga, V. Holten, and B. Widom, "Deriving second osmotic virial coefficients from equations of state and from experiment," *J. Phys. Chem. B* **119**, 13391-13397 (2015).
- ⁷¹ C. A. Cerdeiriñ and B. Widom, "Osmotic second virial coefficients of aqueous solutions from two-component equations of state," *J. Phys. Chem. B* **120**, 13144-13151 (2016).
- ⁷² K. Koga, "Osmotic second virial coefficient of methane in water," *J. Phys. Chem. B* **117**, 12619-12624 (2013).
- ⁷³ M. I. Chaudhari, S. A. Holleran, H. S. Ashbaugh, and L. R. Pratt, "Molecular-scale hydrophobic interactions between hard-sphere reference solutes are attractive and endothermic," *PNAS* **110**, 20557-20562 (2013).
- ⁷⁴ H. S. Ashbaugh, K. Weiss, S. M. Williams, B. Meng, and L. N. Surampudi, "Temperature and pressure dependence of methane correlations and osmotic second virial coefficients in water," *J. Phys.Chem. B* **119**, 6280-6294 (2015).
- ⁷⁵ M. I. Kurnaz and J. V. Maher, "Interaction of dilute colloidal particles in a mixed solvent," *Phys. Rev. E* **51**, 5916-5921 (1995).
- ⁷⁶ B. M. Law, J.-M. Petit, and D. Beysens, "Adsorption-induced reversible colloidal aggregation," *Phys. Rev. E* **5**, 5782-5794 (1998).
- ⁷⁷ R. van Roij and B. Mulder, "Demixing versus ordering in hard-rod mixtures," *Phys. Rev. E* **54**, 6430-6440 (1996).
- ⁷⁸ W. G. McMillan and J. E. Mayer, "The statistical thermodynamics of multicomponent systems," *J. Chem. Phys.* **13**, 276-305 (1945).
- ⁷⁹ R. Battino, "The Ostwald coefficient of gas solubility," *Fluid Phase Equilibria* **15**, 231-240 (1984).
- ⁸⁰ E. E. Tucker and S. D. Christian, "A prototype hydrophobic interaction. The dimerization of benzene in water," *J. Phys. Chem.* **83**, 426-427 (1979).
- ⁸¹ P. J. Rossky and H. L. Friedman, "Benzene-benzene interaction in aqueous solution," *J. Phys. Chem.* **84**, 587-589 (1980).
- ⁸² R. Evans, "The nature of the liquid-vapour interface and other topics in the statistical mechanics of non-uniform, classical fluids," *Adv. Phys.* **28**, 143-200 (1979).
- ⁸³ V. Talanquer and D. W. Oxtoby, "Nucleation of bubbles in binary fluids," *J. Chem. Phys.* **102**, 2156-2164 (1995).
- ⁸⁴ V. Talanquer, C. Cunningham, and D. W. Oxtoby, "Bubble nucleation in binary mixtures: A semiempirical approach," *J. Chem. Phys.* **114**, 6759-6762 (2001).
- ⁸⁵ D. V. Matyushov and B. M. Ladanyi, "Cavity formation

- energy in hard sphere fluids: An asymptotically correct expression," *J. Chem. Phys.* **107**, 5815-5820 (1997).
- ⁸⁶ M.-E. Lee and N. F. A. van der Vegt, "Molecular thermodynamics of methane solvation in tert-butanol-water mixtures," *J. Chem. Theory Comput.* **3**, 194-200 (2007).
- ⁸⁷ Q. Zheng, D. J. Durben, G. H. Wolf, and C. A. Angell, "Liquids at large negative pressures: Water at the homogeneous nucleation limit," *Science* **254**, 829-832 (1991).
- ⁸⁸ M.E.M. Azouzi, C. Ramboz, J.-F. Lenain, F. Caupin, "A coherent picture of water at extreme negative pressure," *Nat. Phys.* **9**, 38 (2013).
- ⁸⁹ G. M. Schneider, "Phase Behavior and Critical Phenomena in Fluid Mixtures under Pressure," *Ber. Bunsenges. Phys. Chem.* **76**, 325-331 (1972).
- ⁹⁰ T. Moriyoshi, T. Sakamoto, and Y. Uosaki, "(Liquid+liquid) equilibria of (water+ ethanol+a C8 alkanol) from 0.1 to 200 MPa at 298.15 K," *J. Chem. Thermodynamics* **21**, 947-954 (1989).
- ⁹¹ J. Aubry, F. Ganachaud, J.-P. Cohen Addad, B. Cabane, "Nanoprecipitation of polymethylmethacrylate by solvent shifting: 1. boundaries," *Langmuir* **25**, 1970-1979 (2009).
- ⁹² R. Botet and K. Roger, "How do interactions control droplet size during nanoprecipitation?," *Curr. Opin. Colloid Interface Sci.* **22**, 108-112 (2016).
- ⁹³ M. Blander, J. Katz, "Bubble Nucleation in Liquids," *AIChE J.* **21**, 833 (1975).
- ⁹⁴ L.A. Turski and J.S. Langer, "Dynamics of a diffuse liquid-vapor interface," *Phys. Rev. A* **22**, 2189 (1980).
- ⁹⁵ M. Kahlweit, G. Busse and J. Jen, "Adsorption of amphiphiles at water/air interfaces," *J. Phys. Chem.* **95**, 5580-5591 (1991).
- ⁹⁶ G. Vazquez, E. Alvarez, J.M. Navaza, "Surface tension of alcohol+water from 20 to 50 °C," *J. Chem. Eng. Data* **40**, 611-614 (1995).
- ⁹⁷ Y. F. Yano, "Correlation between surface and bulk structures of alcohol-water mixtures," *J. Colloid Interface Sci.* **284**, 255-259 (2005).
- ⁹⁸ S. Enders and H. Kahl, "Interfacial properties of water+alcohol mixtures," *Fluid Phase Equilibria* **263**, 160-167 (2008).
- ⁹⁹ A. Fiore, V. Venkateshwaran, and S. Garde, "Trimethylamine N-oxide (TMAO) and tertbutyl alcohol (TBA) at hydrophobic interfaces: Insights from molecular dynamics simulations," *Langmuir* **29**, 8017-8024 (2013).
- ¹⁰⁰ A. Onuki, S. Yabunaka, T. Araki, and R. Okamoto, "Structure formation due to antagonistic salts," *Curr. Opin. Colloid Interface Sci.* **22**, 59-64 (2016).
- ¹⁰¹ S. Yabunaka and A. Onuki, "Electric double layer composed of an antagonistic salt in an aqueous mixture: Local charge separation and surface phase transition," *Phys. Rev. Lett.* **119**, 118001 (2017).
- ¹⁰² H. C. Longuet-Higgins and B. Widom, "A rigid sphere model for the melting of argon," *Mol. Phys.* **8**, 549-556 (1964).
- ¹⁰³ N. F. Carnahan and K. E. Starling, "Intermolecular repulsions and the equation of state for fluids," *AIChE Journal* **18**, 1184-1189 (1972).
- ¹⁰⁴ Y. S. Wei and R. J. Sadus, "Equations of state for the calculation of fluid-phase equilibria," *AIChE Journal* **46**, 169-196 (2000).